Experimental investigations of flame interaction in multi-burner arrays with lean-lifted spray flames

Zur Erlangung des akademischen Grades eines
DOKTORS DER INGENIEURWISSENSCHAFTEN
(DR.-ING)
von der KIT-Fakultät für Chemieingenieurwesen und
Verfahrenstechnik des
Karlsruher Instituts für Technologie (KIT)
genehmigte

DISSERTATION

von

Mohamed Shamma, M.Sc.
aus Mansoura (Ägypten)

Tag der mündlichen Prüfung:	25. November 2024
Erstgutachter:	Prof. Dr.-Ing. Dimosthenis Trimis
Zweitgutachter:	Prof. Dr. Antonio Andreini

To the soul of my beloved brother Mahmoud.

Preface

This work presents the findings of my research on reducing emissions from aircraft engines, conducted during my time at the Engler-Bunte Institute (EBI) at the Karlsruhe Institute of Technology (KIT). My time at KIT has been both an extraordinary professional and personal journey. I had the privilege of collaborating with remarkable individuals and participating in enriching courses, which have greatly contributed to my growth.

I would like to express my deepest gratitude to my supervisor, Prof. Dr.-Ing. Dimosthenis Trimis, for his strong confidence in my ability to undertake this project, as well as for his continuous support, encouragement, and insightful guidance throughout my research. My sincere thanks also go to Dr. Stefan Harth, whose exceptional professional guidance and positive attitude were crucial to my postgraduate studies. I am also deeply appreciative of Dr. Björn Stelzner for his assistance, particularly in operating the measurement systems.

I would like to acknowledge the support from my colleagues—Thomas von Langenthal, Sebastian Schulz, Michal Fedoryk, and Petra Weinbrecht—who made my time at KIT both productive and enjoyable. Additionally, I extend my sincere appreciation to the administration and technical staff of the Engler-Bunte Institute (EBI) for creating a supportive and conducive work environment.

Finally, I owe my deepest gratitude to my family, who have been my foundation throughout my academic journey. I am especially thankful to my father, who ignited my passion for academic research and ultimately inspired

me to pursue my Ph.D. Their encouragement, kindness, and constant support have been instrumental in my success. I am particularly grateful for the love and support of my mother, my wife, and my daughter, Masa.

Karlsruhe, November 2024 Mohamed A. Shamma

Acknowledgements

This project has received funding from the Clean Sky 2 Joint Undertaking (JU) under grant agreement No. 831881 (CHAiRLIFT). The JU receives support from the European Union's Horizon 2020 research and innovation programme and the Clean Sky 2 JU members other than the Union. The author gratefully acknowledge the German Research Foundation (DFG) for the financial support of measuring instruments within the HBFG program (INST 121384/178-1 FUGG).

Abstract

Lean burn in gas turbine technology has drawn a lot of interest recently as a way to lower emissions from combustion systems. With lean combustion, a larger amount of air is fed into the combustion chamber compared to the amount of fuel, resulting in a leaner fuel-air mixture. This enables to control of the combustion temperature and delimits the nitric oxides (NOx). These advantages may result in less fuel use, lower operational costs, and a lesser environmental footprint. However, lean combustion can also pose challenges, such as unstable flame behavior or periodic variations in pressure and temperature within the combustion chamber, which can cause damage to the gas turbine. These challenges must be carefully considered and addressed in the design and operation of gas turbines using lean combustion technology to realize the full potential of this technology. A novel combustor concept that integrates lean combustion, low swirl, lifted flame, and a helical burner arrangement is presented in this research. The combination of these techniques offers potential improvements in terms of mechanical and thermal performance.

The main objective of current study is to provide experimental results on the baseline configuration of the innovative CHAIRLIFT combustor concept, which can be used to identify/understand the relevant phenomena i.e. related to the stability limits, emission performance and flame structure. Lean lifted spray flames and their very low nitrogen oxides emissions are combined with an inclination of burners in annular combustor leading to a more compact combustor. CHAIRLIFT combustor concept is based on “low swirl” lean lifted spray flames, which features a high degree of premixing and consequently significantly reduced nitrogen oxides emissions and flashback risk compared to conventional swirl stabilized flames. In the CHAIRLIFT combustor concept, the lifted flames are combined with Short Helical Combustors (SHC) arrangement to attain stable combustion by tilting the axis of the flames relative to the axis of the turbine to enhance the interaction of adjacent flames in a circumferential direction. A series of experimental tests were conducted at a multi-burner array test rig consisting of up to five modular burners at different burner inclination angles, equivalence ratios (ϕ), different relative air pressure drop across the nozzle ($\frac{\Delta p}{p}$), and varied air inlet temperature T_{Air} at ambient pressure. For all investigated configurations, good stability limits for non-piloted burners was observed. The inline and inclined have better stability range compared moderate swirl by previous investigations. A slightly higher stability was observed for the inline arrangement compared to the inclined arrangement due to local flow exchange at higher temperature level. The unwanted flow deflection of highly swirled flames in Short Helical Combustors arrangement could be avoided with the investigated low swirl lifted flames. Moreover, the flame chemiluminescence (OH*) measurements were used to provide a qualitative characterization of the flame topology. Moreover, exhaust gas measurements at the inline and

the inclined multi-burner configuration was performed, showing that the nitric oxides emissions (NOx) are at the expected low range for such lifted flames compared to previous investigations and the inclined arrangement has a better emissions performance for most operating conditions due to higher lift off height. The ion probe measurement system was installed at the inclined multi-burner array to investigate if conditions near to LBO can be detected by certain parameters. The increase of timescale of the ion current fluctuations was identified as suitable indicator.

The results show that a remarkable high stability of the low swirl and lifted flames was observed compared to moderate swirl flames with larger inner recirculation zone. The study highlights the significant influence of fuel droplet evaporation time on flame stability near the flame root under low air inlet temperatures. Moreover, the complex flame stability mechanism in inclined configurations is found to be controlled by various parameters, such as outer recirculation zone size, air inlet temperature, and additional vortices generated by pressure differences near the wall. A slightly higher stability was observed for the inline arrangement compared to the inclined arrangement and different stabilization mechanism and flame structure at different air inlet temperature was explained in details. Exhaust gas analyses were performed for the multi-burner arrangement emissions. It was observed that, these lifted flames provide very low NOx emissions over a wide range of operating conditions for all in- vestigated configurations. These findings have important implications for the future development and optimization of lean combustion technology for aircraft engines.

Contents

List of Figures

List of Tables

Nomenclature

Roman Symbols

A	Area	[m^2]
C	Concentration	[mol/m^3]
F	Force	[N]
m	Mass	[kg]
P	Pressure	[Pa]
R	Universal Gas Constant	[J/(mol·K)]
SMD	Sauter Mean Diameter	[mm]
SN	Swirl Number	[-]
T	Temperature	[K]
U	Velocity	[m/s]
V	Volume	[m^3]
FN	Flow Number	[$kg/h/\sqrt{bar}$]
EI	Emission Index	[kg/kg_{fuel}]

Greek Symbols

α	Thermal Diffusivity	[m^2/s]
β	Volumetric Expansion Coefficient	[1/K]
δ_{th}	Thermal Thickness (Thickness of the Reaction Zone)	[mm]
ϵ	Turbulent Dissipation Rate	[m^2/s^3]
η	Efficiency	[-]
κ	Specific Heat Ratio (c_p/c_v)	[-]
λ	Air-to-Fuel Ratio	[-]
μ	Dynamic Viscosity	[Pa·s]
ν	Kinematic Viscosity	[m^2/s]
ϕ	Equivalence Ratio	[-]
ρ	Density	[kg/m^3]
σ	Surface Tension	[N/m]
τ	Time Constant	[s]
ω	Angular Velocity	[rad/s]

Superscripts

$(...)'$	Fluctuation
$\overline{(...)}$	Average
$(...)^*$	Excited-State Radical

Subscripts

$(...)_1$	In the Plenum
$(...)_2$	In the Combustor
$(...)_{ad}$	Adiabatic

$(...)_{eff}$	Effective
$(...)_{f}$	Fuel
$(...)_{Air}$	Air
$(...)_{pr}$	Primary Swirler
$(...)_{sec}$	Secondary Swirler
$(...)_{theo}$	Theoretical
$(...)_{tot}$	Total
$(...)_{Isentropic}$	Isentropic

Acronyms

AFR	Air-Fuel Ratio
CAEP	Committee on Aviation Environmental Protection
CHAIRLIFT	Compact Helical Arranged CombustoRs with Lean LIFTed Flames
CO	Carbon Monoxide
CO_2	Carbon Dioxide
CxHy	General Chemical Formula for a Hydrocarbon Fuel
Da	Damköhler Number
EI	Emission Index [kg/kg_{fuel}]
HS	High Speed
ICAO	International Civil Aviation Organization
IRZ	Inner Recirculation Zone
JET-A1	Jet Fuel Type A1
Ka	Karlovitz Number

LBO	Lean Flame Blowout	
LOH	Lift-Off Height	
LTO	Landing and Take-Off Cycle	
NGV	Nozzle Guide Vanes	
NO_x	Nitrogen Oxides ($NO_x = NO + NO_2$)	
N_2O	Nitrous Oxide	
OGV	Outlet Guide Vanes	
OPR	Overall Pressure Ratio	
ORZ	Outer Recirculation Zone	
PIV	Particle Image Velocimetry	
ppm	Parts Per Million	
Re_t	Turbulent Reynolds Number	
SHC	Short Helical Combustor	
SL	Laminar Flame Speed	
SO_x	Sulfur Oxides	
SMD	Sauter Mean Diameter	[mm]
T_{burnt}	Adiabatic Burned Gas Temperature	[K]
$T_{unburnt}$	Temperature of the Unburned Gases	[K]
UV	Ultraviolet	
UHC	Unburned Hydrocarbon	
$\frac{\Delta p}{p_1}$	Relative Air Pressure Drop Across the Nozzle	[-]
$\dot{D}$	Axial Flux of Angular Momentum	[N·m]
$\dot{I}$	Axial Flux of the Axial Momentum	[N]

τ_c	Chemical Time Scale	[s]
τ_t	Turbulent Integral Time Scale	[s]
δ_{th}	Thermal Thickness (Thickness of the Reaction Zone)	[mm]
U_{inf}	Inflow Velocity	[m/s]
η_κ	Kolmogorov Scale	[mm]
Al_2O_3	Aluminum Oxide	
A_r	Nozzle-Combustor Expansion Area Ratio	[-]

Chapter 1

Introduction

The historical evolution of energy resources used by mankind has been characterized by dramatic shifts over the course of several centuries. In the eighteenth and nineteenth centuries, wood stood as the predominant energy source, providing the primary fuel for a wide range of applications. The subsequent eras witnessed the ascendancy of coal and oil, propelling industrialization and global energy consumption to remarkable levels. However, the late twentieth century marked a pivotal moment with the rise of nuclear power as a prominent contributor to the global energy matrix. This technological milestone was further complemented by the emergence of renewable energy sources at the start of the twenty-first century, indicating a significant shift toward sustainable energy supply.

Nonetheless, since the inception of the industrial revolution, fossil fuels, including coal, oil, and natural gas, have undeniably played a preeminent role

as the cornerstone of global energy supply. Fossil fuels have been instrumental in meeting the ever-expanding global energy demand, powering industries, transportation, and the vital functions of modern society. Remarkably, despite the growing interest in renewable energy alternatives and the imperatives of sustainability, fossil fuels are expected to remain the dominant energy source in the foreseeable future. This trajectory is highlighted by empirical data, as elucidated in Fig. 1.1.

Therefore, providing efficient and environmentally clean power generation has become increasingly important due to the rising cost of fossil fuels, more stringent emissions regulations, and increasing demand for energy. In this context, enhancing combustion devices in terms of energy efficiency and pollution reduction is critical for next-generation engines. The issue of pollutant emissions, particularly from aeronautic engines, has emerged as a subject of heightened societal concern. The environmental impacts of these

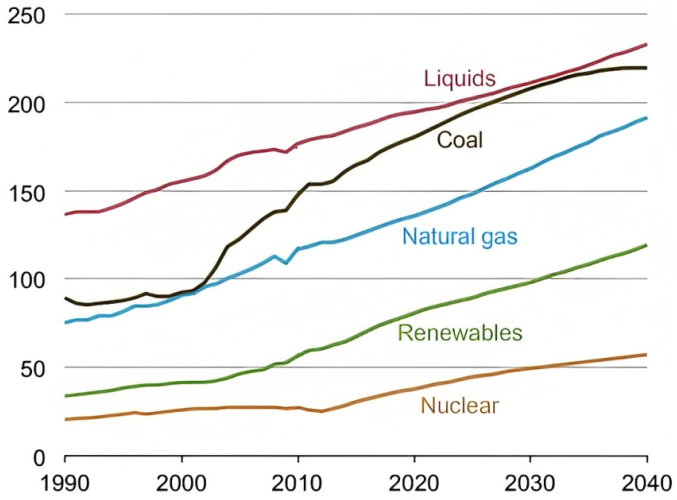

Figure 1.1: World energy consumption by fuel type [3].

emissions extend across multiple domains, encompassing both land-based and atmospheric realms.

The spectrum of pollutants encompasses nitrogen oxides (NO_x), unburned hydrocarbons (UHC), carbon monoxide (CO), sulfur oxides (SO_x), and particulate matter [4]. The critical attributes of these emissions reside in their harmful properties and potential for significant impacts on human health, the environment, and biological ecosystems. The NO_x emissions, comprising nitric oxide (NO), nitrogen dioxide (NO_2), nitrous oxide (N_2O), and their derivatives, exerts a diverse array of impacts on both health and environmental systems. Nitric oxide (NO), due to its low solubility in water, possesses the ability to permeate the respiratory system, while nitrogen oxides can disrupt lung structures and functions by diffusing through alveolar cells. Nitrous oxide (N_2O), recognized as a potent greenhouse gas, persists in the atmosphere for over a century, exerting a warming effect per molecule that is 300 times greater than that of carbon dioxide. Even at concentrations as low as 300 parts per billion, nitrous oxide (N_2O) contributes to Earth's warming by 0.1 W/m^2 [5].

Regulatory stipulations, as mandated by the International Civil Aviation Organization (ICAO), constitute a paramount impetus for the ongoing development and enhancement of combustor technologies, particularly in the realm of emissions reduction. These guidelines, formulated to reduce engine emissions, are established under the authority of the Committee on Aviation Environmental Protection (CAEP). The specific allowable levels of NO_x emissions for jet engines are outlined in Annex 16 Volume II to the Convention on International Civil Aviation. [6]. Notably, the prescribed levels depend on the engine's overall pressure ratio (OPR) and its thrust

generation capacity. As the OPR increases, the permissible amount of NO_x also increases. A visual representation of the defined limits set by CAEP for aero-engines, along with a comparative assessment of emissions from selected exemplary engines, is elucidated in Fig. 1.2. Currently, a substantial fraction of aero-engines effectively operates within the boundaries stipulated by CAEP's sixth set of emissions limits. These emission levels are determined through standardized testing conducted during the landing-takeoff (LTO) cycle, as illustrated in Fig. 1.3. However, as future emissions limits are projected to decrease, engines operating within current limits may no longer meet certification standards [7].

According to the Advisory Council of Aeronautics Research in Europe's (ICAO) goal for 2020, emissions of CO_2 and NO_x must be reduced by 50% and 80%, respectively, compared to those permitted under CAEP 2. While

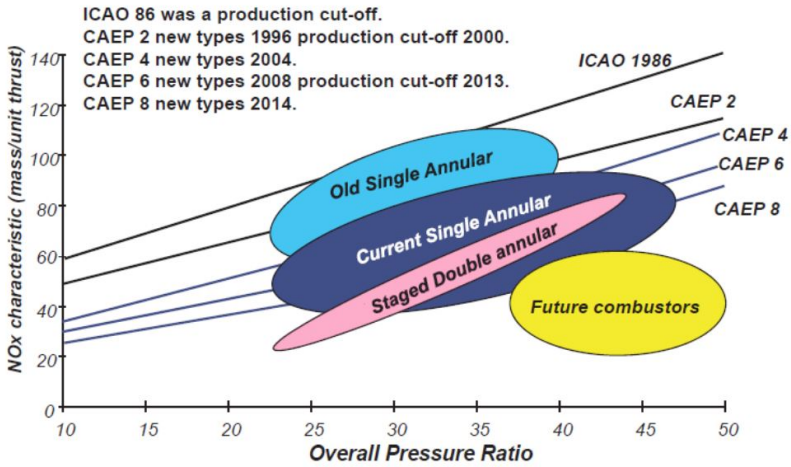

Figure 1.2: Allowed mass in grams of NO_x emissions per rated output depending on the overall pressure ratio of the jet engine [4].

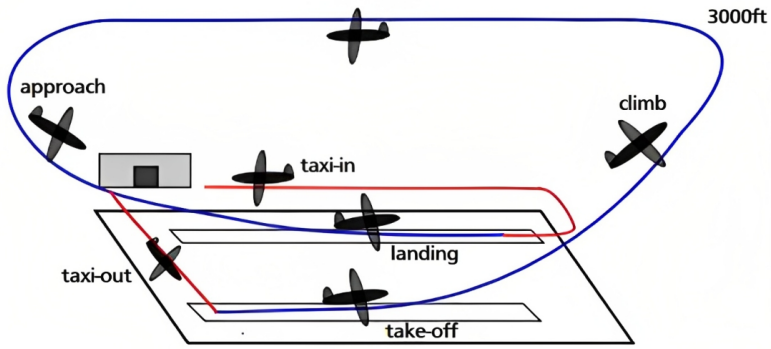

Figure 1.3: ICAO LTO Cycle with standard power settings during engine certification: 26 minutes taxi (7 % take-off thrust), 42 seconds take-off (100 % take-off thrust), 132 seconds climb (85 % take-off thrust) and 4 minutes approach (30 % take-off thrust).

some of these savings will be attained by lowering fuel usage overall, about 50% will come from improving the combustor. Fig. 1.2 also displays the benchmark for these reductions.

The harmful impact of NO_x emissions on the environment and human health makes it crucial to reduce them in combustion processes. To develop effective strategies for NO_x reduction, it is essential to understand the formation mechanisms of NO_x. Three primary mechanisms have been identified for NO_x formation: Thermal NO_x, Prompt NO_x, and Fuel NO_x [8]. Thermal NO_x is produced by the Zeldovich mechanism [9], which grows exponentially with temperature. As a result, low temperature, low O_2 concentration, and short residence time are key criteria for lowering thermal NO_x. Prompt NO_x, also known as Fenimore NO_x, forms during the initial stages of combustion when the fuel molecules break down into smaller, reactive species such as hydrocarbon radicals. These species react with nitrogen and oxygen or oxygen containing species to form NO_x. Fuel NO_x generates during combustion when nitrogen-containing compounds in the fuel react with oxygen to form NO_x.

This reaction occurs when the fuel contains chemically bonded nitrogen in the form of amines, nitro compounds, or other nitrogen-containing compounds.

The lean premixed combustion technique is employed to mitigate the formation of thermal and prompt NO_x during the combustion process. Well premixed lean air-fuel mixtures result in reduced combustion peak temperatures, which in turn reduces the production of thermal NO_x.

The purpose of this research is to introduce a novel combustor concept aimed at reducing NO_x emissions while maintaining a wide range of flame stability. Lean combustion can be employed in this perspective [10], but accurate control of local temperature is required in order to contain emission levels of other pollutant species and to ensure the required stability range [11]. Lean premixed combustion has also been considered an essential technology for achieving ultra-low emissions in aero-engines. This technology involves the mixing of fuel and air prior to combustion, resulting in a more uniform and complete combustion process with fewer pollutants emitted. Lean premixed combustion has been shown to achieve significant NO_x reductions, making it a vital technology in meeting emission regulations. Therefore, the development of low-emission combustor concepts for aero-engines has placed significant importance on the advancement of lean premixed combustion technology in recent years.

To maximize the potential of this technology, careful consideration of auto-ignition delay times is essential, especially when using liquid fuels like JET-A1 in aero-engines. Auto-ignition delay time is a critical factor limiting the available residence time for pre-mixing and pre-evaporation.

1.1 Objectives

Gas turbines are widely employed as the primary machinery in various sectors, including power generation, aviation (aero-engines), maritime propulsion, and industrial mechanical systems. Currently, there is a compelling need to enhance gas turbine technology, driven by the aim of achieving better performance and reducing environmental footprint.

The main objective of this Ph.D. thesis is to conduct a comprehensive experimental investigation of an innovative low-emission burner concept designed for aero-engine applications. Developed within the CHAIRLIFT (Compact Helical Arranged combustoRs with lean LIFTed flames) European research project, this burner concept combines two novel features: low swirl lean lifted spray flames to achieve high premixing and significantly reduce NO_x emissions; and the Short Helical Combustor (SHC) arrangement. The SHC involves tilting the flame axes relative to the turbine axis to enhance circumferential flame interaction and aiming to improve combustion stability. Additional benefits are the reduced length of the combustor. This thesis explores the impact of varying the combustor tilt angle on the combustion characteristics. This study explores the impact of varying the combustor tilt angle on the interaction between adjacent flames, using adjustments in the offset between these flames to mimic different tilt angles in the annular combustor setup.

Although lifted flames have been extensively studied, there remains a distinct lack of comprehensive understanding regarding their stabilization mechanisms, particularly in multi-burner configurations. This research project

represents a distinct contribution to the existing literature, focusing specifically on the study of low-swirl lifted flames using liquid fuel in multi-burner domain. To the best of the author's knowledge, this work marks the first experimental investigation into applying this innovative combustion concept with the use of liquid fuel.

To achieve these goals, a series of comprehensive experimental tests employing advanced optical measurement techniques, including Particle Image Velocimetry (PIV), Mie scattering, and OH* chemiluminescence, were conducted. These measurements provided insights into velocity fields, fuel spray properties, and flame structure. Within the experimental setup, local probe invasive measurements were also carried out employing S-type thermocouples and a gas sampling probe, which were affixed to a traverse system. This instrumentation facilitated the quantification of temperature distributions and the concentrations of emission gases at various points within the combustion chamber.

The experimental campaign closely replicated similar real-world aeronautic combustion conditions at ambient pressure with varied tilt angle of burners (θ), and equivalence ratios (Φ), different air mass flow rate defined by relative air pressure drop across the nozzle ($\frac{\Delta p}{p1}$). These conditions were characterized by low swirl levels and the replication of varied air inlet temperatures T_{Air}, reaching up to 673 K at ambient pressure. The research also assessed the potential of the CHAiRLIFT burner concept to reduce NO_x emissions while maintaining flame operation under extremely lean equivalence ratios. Ultimately, the feasibility of integrating the CHAiRLIFT burner concept into aero-engine systems was evaluated and compared to typical higher swirl flames with larger inner recirculation zones, considering its potential

benefits in terms of emissions reduction, enhanced flame stability, and a shorter, lighter combustor.

In summary, this research enhances our understanding of applying this innovative concept to aero-engines, with potential benefits for more efficient and environmentally friendly combustion systems.

1.2 Outline

This thesis is motivated by the aim of evaluating a novel combustor concept designed to achieve low nitrogen oxide emissions, with the potential to align with the long-term emission targets established by European authorities for aircraft engines. To ensure clarity and coherence in presenting the research, the dissertation is structured as follows:

After this introduction chapter explaining the background and motivation for this research, Chapter Two offers a thorough exploration of the theoretical fundamentals and reviews prior research necessary to understand the core concepts of combustion related to this concept.

Chapter Three details the experimental setup and instrumentation, including operational principles and technical specifications. It also discusses the data acquisition setup and specific tools including high-speed cameras, laser diagnostics, ion probe, and thermocouples.

Chapter Four presents experimental results for different combustor configurations including inline and inclined arrangements under various operating conditions like air inlet temperature, air pressure drops across the nozzle,

and equivalence ratios. It compares flame stability with previous studies and analyzes flame topology and emissions.

Chapter Five summarizes the main findings and conclusions of the study, discussing their applicability to real engines. It offers recommendations for future research focused on improving helical arranged combustor, and advancing lean-low swirl combustion technologies.

Chapter 2

State of art

Combustion process represents a fundamental chemical process in which a fuel undergoes rapid oxidation releasing heat and typically accompanied by light, thus playing a pivotal role in numerous energy conversion processes. This process is central to many energy conversion technologies, transforming energy locked within chemical bonds into thermal energy. Specifically, hydrocarbon combustion involves the reaction of hydrocarbon molecules, consisting of hydrogen and carbon, with oxygen to yield carbon dioxide, water, and heat. These hydrocarbons are the main components of traditional fossil fuels such as natural gas, oil, and coal, which are commonly referred to as hydrocarbon resources due to their composition. In addition to traditional fuels, alternative non-fossil fuels, known as drop-in fuels or low-carbon fuels, have recently gained significant interest as a promising medium-term solution to gradually reduce carbon emissions. These fuels are often produced from renewable resources, aiming to reduce dependence on fossil fuels and

lower greenhouse gas emissions. Examples of drop-in fuels include biofuels made from plant materials, synthetic fuels produced from carbon dioxide and hydrogen, and renewable natural gas derived from organic waste. Despite their potential, the development of these alternative fuels and the necessary expansion of fuel infrastructure are still in the early stages, with studies indicating that higher costs and more time will be required for infrastructure development [12].

Combustion is a complex process influenced by various parameters, including air-to-fuel ratio, fuel composition, oxidant concentration, temperature, and pressure. The interaction of these factors not only influences the speed and completeness of the reaction but also affects the production of harmful emission byproducts. A full understanding of these factors is essential for optimizing combustion conditions to achieve lower emissions combustion process. As this study focuses on the combustion of hydrocarbon fuel (Jet A-1 fuel), this introduction chapter will explore the nature of hydrocarbon combustion. The hydrocarbon combustion can occur under various conditions, with specific reaction pathways determined by the aforementioned factors. Regardless of the type of hydrocarbon fuel, combustion with oxygen primarily results in the production of carbon dioxide, water, and heat. This general reaction is illustrated in the following equation, representing the stoichiometric complete conversion of a hydrocarbon fuel:

$$C_xH_y + \left(x + \frac{y}{4}\right)O_2 \longrightarrow xCO_2 + \frac{y}{2}H_2O + Heat \qquad (2.1)$$

where C_xH_y is the hydrocarbon fuel, $\left(x + \frac{y}{4}\right) O_2$ is the stoichiometric amount of oxygen, xCO_2 is the carbon dioxide produced, $\frac{y}{2}H_2O$ is the water vapor produced, and Heat represents the energy released.

The theoretical background in this chapter is referenced from [10–22]. More specific citations will be included where relevant.

2.1 Flames in Laminar Flows

For laminar flames issuing from a tube burner, two models of combustion are depicted in Fig. 2.1, based on the mixing of fuel and oxidizer: laminar premixed flames and laminar non-premixed flames.

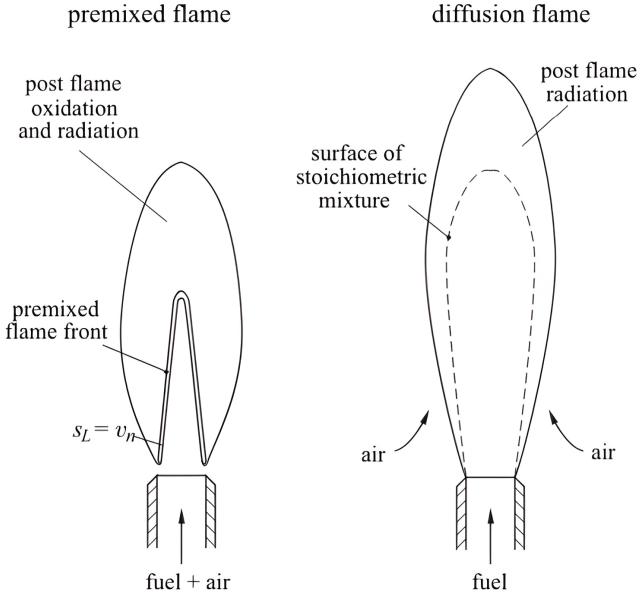

Figure 2.1: Different modes of laminar combustion [23].

Laminar premixed flames are characterized by a steady and predictable flame front that propagates through the fuel-oxidant mixture at a constant speed. The flame front is thin and well-defined, exhibiting a high temperature gradient that results in a sharp increase in temperature across the flame front. In the case of a Bunsen burner, where fuel and air are premixed within the tube and ignited downstream, the premixed flame front propagates toward the burner until it stabilizes in the form of the well-known Bunsen cone. The key characteristic of this combustion mode is the laminar burning velocity, which is the rate at which the flame front moves normal to itself into the unburned mixture. In a steady state, the burning velocity must match the flow velocity.

The structure of laminar flames is influenced by several factors, including fuel type, oxidant concentration, and temperature. The reaction kinetics in these flames are well-defined, and the flame speed is primarily governed by the fuel-oxidant concentration, reaction rate, and diffusion process. Investigating the structure of laminar premixed flames is crucial to understanding combustion characteristics. However, experimental investigations is challenging due to the very thin reaction zone. To address these challenges, various theoretical and numerical approaches have been developed. Historical theoretical analyses include the Thermal Theory proposed by Mallard and Le Chatelier [24] and Damköhler [25], the Diffusion Theory by Tanford and Pease [26], and the Combined Theories by Zeldovich [27]. Moreover, since the 1980s, numerical calculations have played a significant role, with programs like CHEMKIN [28] being used to solve balance equations and analyze the dynamics of laminar premixed flames. The structure of premixed laminar flames can be analyzed computationally for most fuels, encom-

passing temperature and species concentration profiles. An example of a computed composition and temperature profiles through a one-dimensional adiabatic premixed laminar flame is shown in Fig. 2.2. The flame structure is composed of four zones: the cold reactants zone, the preheat zone, the reaction zone, and the products zone. The preheat zone is predominantly characterized by heat conduction and mass diffusion of the reactants, while the reaction zone is dominated by chemical reaction and mass diffusion. The reactants are initially at the unburned gas temperature, $T_{unburnt}$. The temperature gradually increases in the preheat zone due to conductive heat transfer from the reaction zone, until the adiabatic burned gas temperature, T_{burnt}, is achieved in the product zone. The temperature profile is nonlinear due to the nonlinear heat release and transport processes. The continuous heating of the reactants leads to their reaction at an increasing rate. The flame thickness, a characteristic length scale of a flame, is defined as the thickness of the reaction zone. Flame thickness is calculated in terms of the thermal thickness δ_{th} [13]:

$$\delta_{th} \equiv \frac{\max(T) - \min(T)}{\max\left(\left|\frac{\partial T}{\partial n}\right|\right)} \tag{2.2}$$

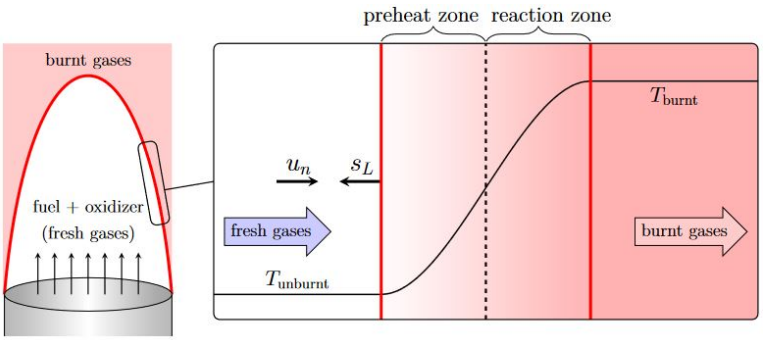

Figure 2.2: Schematic diagram of laminar premixed flame, reproduced from [29].

where $\frac{\partial T}{\partial n}$ is the temperature gradient inside the flame front in its normal direction. If the flame is in steady state, it burns with the same speed s_L towards the fresh gases as it is convected away by the flow with u_n, which is the gas velocity of the fresh gases normal to the flame front. The burning velocity or flame speed s_L is a fundamental parameter that determines the flame's propagation speed against the fresh gas. Flame speeds are critical for predicting the heat release rate, and flashbacks, making them a crucial factor in the combustion process [13]. The chemical time scale or flame transit time τ_c is defined as:

$$\tau_c \equiv \delta_{th} / s_L \tag{2.3}$$

The flame temperature primarily governs the formation of pollutants in laminar flames, making controlling the flame temperature essential in reducing pollutant emissions.

In the case of *Laminar non-premixed flames*, fuel and air are supplied separately into the combustion zone. The mixture then undergoes convection and diffusion processes before a chemical reaction occurs, as illustrated on the right-hand side of Fig. 2.1. The fuel is injected through the tube, and during combustion, it mixes with the surrounding air primarily through convection and diffusion.

For non-premixed flames, combustion typically occurs near the stoichiometric mixture fraction. This critical region is where fuel and air are locally mixed in precise proportions, facilitating the complete consumption of both components. Achieving these conditions results in the high flame temperatures and, owing to the temperature sensitivity of the chemical reactions, fast reaction rates.

In non-premixed combustion modeling, the approach focuses on the solution of transport equations for one or two conserved scalars, typically the mixture fractions, without directly solving the equations for individual species. Instead, species concentrations are derived from these predicted mixture fraction fields, which simplifies the modeling process significantly. The mixture fraction plays a central role in this approach. It represents the mass fraction originating from the fuel stream and includes the local mass fractions of both burnt and unburnt elements across all products. This parameter is essential because it captures the conserved nature of atomic elements in chemical reactions. As such, the mixture fraction is a conserved scalar quantity; its governing transport equation lacks a source term, which greatly simplifies the complexity of the modeling process.

2.2 Flames in Turbulent Flows

Turbulent flames are characterized by a highly unsteady and chaotic flame front that fluctuates rapidly in response to the turbulent flow field. Turbulence is characterized by a broadband of fluctuations of the fluid velocity. In turbulent flows, large eddies are generated which break down in size until they dissipate their kinetic energy into heat (energy cascade), shown in Fig. 2.3. The characteristic length scale of the large, energy carrying eddies is the integral length scale L_t. The smallest eddies reach the Kolmogorov length η before dissipating.

The turbulent flame front is typically thick and wrinkled, with a low average temperature gradient, resulting in a gradual increase in temperature across

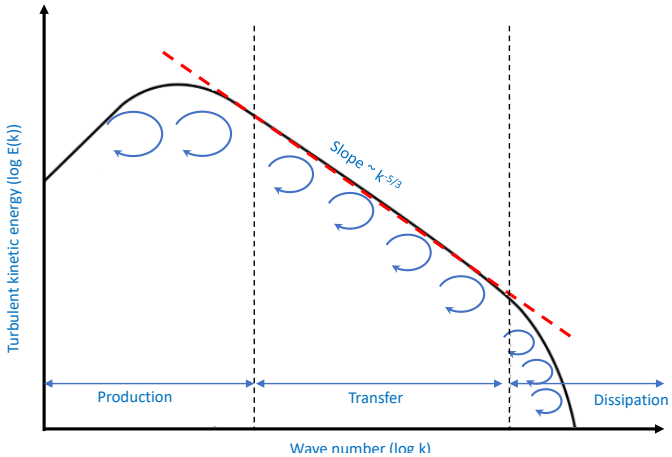

Figure 2.3: Turbulent energy cascade.

the flame front. The turbulent flame structure is influenced by various factors, including the turbulence intensity, and chemical kinetics. In turbulent combustion, eddies stretch the flame front leading to an increase in flame surface area compared to a laminar flame and therewith an increased volumetric heat production.

Various academic studies have explored turbulent combustion, focusing on both premixed and non-premixed turbulent combustion regimes. For turbulent premixed combustion, the Borghi diagram stands out as the most recognized framework. Originally proposed by Borghi [31] and later modified by Peters [32], this diagram categorizes the premixed turbulent combustion into four different regimes. In the Borghi diagram, the depiction of premixed combustion relies fundamentally on the ratios of several critical length and time scales. These include the integral length scale (l_I), the thickness of the laminar flame (δ_l), the root mean square (rms) of velocity fluctuations (u'_0), and the laminar flame speed (s_l). The interrelationships of these scales

are quantified by various dimensionless numbers, which serve to classify different combustion regimes depicted within the diagram.

The Damköhler number (Da) illustrates the ratio between the turbulent integral time scale (τ_t) and the chemical reaction time scale (τ_c). Meanwhile, the Karlovitz number (Ka) relates the time scales of the smallest eddies in turbulence to the chemical time scales, expressed as the ratio between the thickness of the laminar flame and the Kolmogorov scale (η_K). Another important parameter is the turbulent Reynolds number (Re_t). The regimes within the turbulent premixed combustion are distinguished based on these non-dimensional numbers, as shown in Fig. 2.4 as:

Laminar Combustion Zone: Positioned at the beginning of the diagram in Fig. 2.4, this region exhibits no interaction between turbulence and the flame, dominated by the presence of laminar flamelets and marked by $Re_t < 1$.

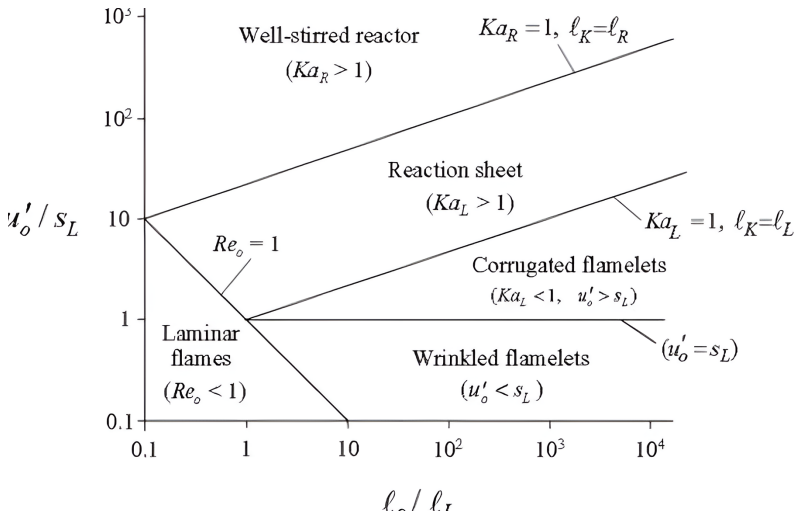

Figure 2.4: Borghi Diagram for premixed combustion regimes [30].

Flamelet Domain: Identified where $Ka < 1$ and $Re_t > 1$, this domain is characterized by chemical time scales that are shorter than those of the turbulent flows, resulting in a Damköhler number $Da < 1$.
Thickened-Wrinkled Flame Domain: This region, defined for $1 < Ka \leq 100$, is also known as the thin reaction zone. In this domain, the smallest turbulent structures can impact the flame's preheat zone without altering the core reactions.
Thickened Flame Domain:, where $Ka > 100$ and $Da < 1$, shows significant turbulence interaction with the reaction zone, leading to possible local extinctions and a lack of identifiable laminar flame structures.
According to Poinsot and Veynante [13], creating a diagram for turbulent non-premixed combustion is more challenging than for premixed regimes. This difficulty arises because the diffusion flames in non-premixed combustion heavily depend on specific flow conditions, lacking well-defined length, time, and velocity scales. These complexities make the precise classification and diagram construction of turbulent flame regimes challenging. To address these issues, additional assumptions are often needed to bridge the gaps between various flame/turbulence scales. Key metrics used in this classification include the mean scalar dissipation rate and the local flame Damköhler number, which relates the characteristic and chemical time scales.

Turbulent non-premixed combustion can be classified into different regimes based on the relationships between specific non-dimensional numbers, including the Turbulent Reynolds Number, Mean Scalar Dissipation Rate, and Local Flame Damköhler Number. Mean Scalar Dissipation Rate is used to estimate the diffusion time scale τ_f. The Local Flame Damköhler Num-

ber (Da^{fl}) is defined as the ratio of the characteristic time scale τ_f to the chemical time scale τ_c, and the Turbulent Reynolds Number (Re_t).

These regimes are defined as described in Fig. 2.5 as follows:

Laminar Combustion Region: Characterized by laminar flamelets, with $Re_t < 1$.
Laminar Flamelet Assumption: Confined by $Da^{fl} = Da^{LFA}$ and $Re_t = 1$.
Flame Extinction Zone: Identified where $Da^{fl} = Da^{ext}$, occurring at large chemical times τ_c.

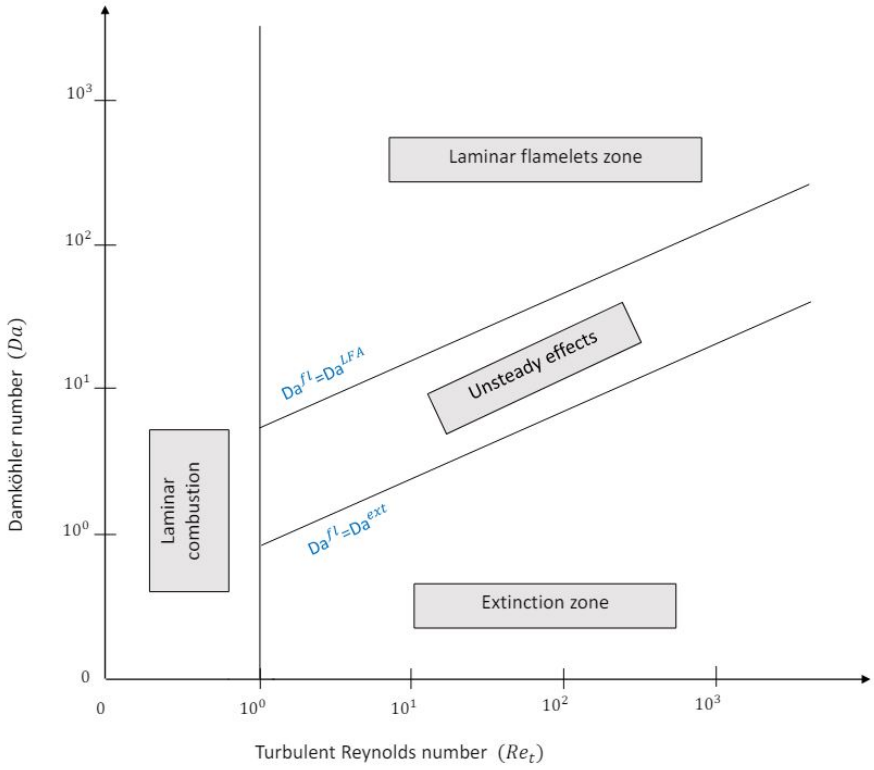

Figure 2.5: Non-Premixed combustion regimes [30].

2.3 Overview of CHAIRLIFT combustor concept

Flame stability is a crucial parameter that dictates the operational reliability and safety of a system. Optimal flame stability ensures controlled combustion rates, minimizing the risks of blowout and a steady heat release output. To achieve these objectives, this research introduces an innovative combustor design, CHAIRLIFT (Compact Helical Arranged combustoRs with Lean Low Swirl Lifted Flames). This design could have impact on flame stability and combustion emissions.

The combustor concept examined in this study leverages several combustion phenomena, including the utilization of lifted flames, the application of low swirl techniques, and the adoption of lean combustion strategies in a tilted burner arrangement called short helical combustor arrangement (SHC). SHC has been analytically investigated by Ariatabar et al.[33]. As shown in Fig. 2.6. The tilting angle of the burner induces recirculation within the combustion chamber, facilitating the transfer of hot combustion products between adjacent burners. Additionally, the SHC provides several mechanical advantages over conventional combustors, such as a reduced combustor length, fewer Outlet Guide Vanes (OGVs) and Nozzle Guide Vanes (NGVs), and consequently, lower total pressure losses and cooling air requirements. Further details of this concept will be discussed in Section 2.3.4.

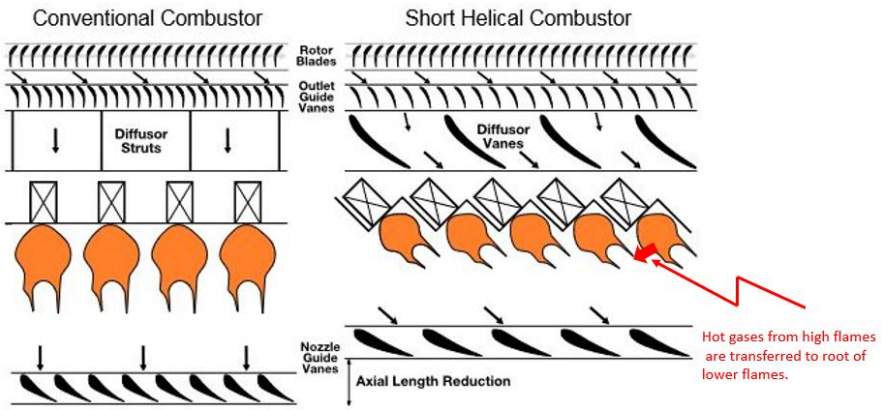

Figure 2.6: Comparison of the SHC and conventional combustor alignment reproduced from [33].

The current research aims to investigate the impact of utilizing this concept on the combustion characteristics, including flame stability, flame structure, and the main emissions. In the subsequent subsections, a detailed overview of each phenomenon associated with this innovative concept will be presented.

2.3.1 Lifted flames

In general, stable combustion conditions can only be achieved within flammability limits and a balance between inflow velocity U_{inf} and flame/reaction speed. The speed of the reaction is typically characterized by the laminar flame speed S_L. As shown in Fig. 2.7, the relationship between flow velocity and flame spped could be classified as follows:

- **Flashback**: When the flame speed exceeds the inlet velocity, flashback occurs, causing the flame to move upstream into the burner or fuel supply system.

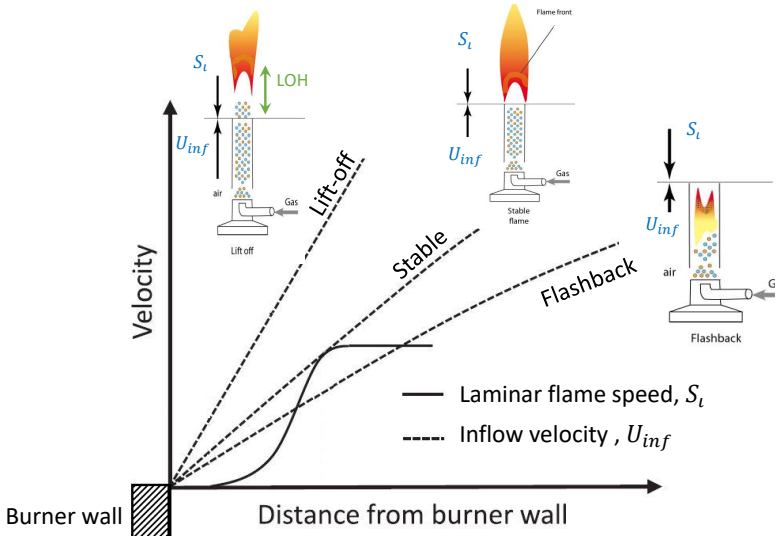

Figure 2.7: Critical velocity gradient model showing the flow velocity and burning velocity profiles, reproduced from [1, 2].

- **Stable**: when both speeds are equal but in opposite directions. At this point, the flame front is perpendicular to the streamline.
- **Lift-off**: If the flame speed is lower than the flow velocity, the flame will move downstream and lift off the burner exit.

The primary feature of lifted flames is their ability to detach from the nozzle outlet. This reduces the risk of flame flashback in premixed flames and allows for a high degree of premixing in non-premixed flames. Lifted flames have the advantage of avoiding direct contact between hot reaction zone and the nozzle, diminishing the thermal load on the combustor components.

Many studies have been conducted to investigate flame stabilization mechanisms for laminar and turbulent lifted flames. For a fundamental under-

standing of non-premixed lifted jet flames, the stabilization mechanism of a laminar lifted flame was first explained schematically by Chung and Lee [34], which generally exhibit a tribrachial edge flame structure that consists of rich/lean premixed flame wings and a trailing non premixed flame in between along the isoline of the stoichiometric mixture fraction. The intersecting point of the three branches is called 'tribrachial (triple) point', and the flamebase of a lifted jet flame typically lies at this point [35]. The stabilization of non-auto ignited lifted jet flames is controlled by kinematic balance between the propagation speed of a lifted flamebase and an upcoming flow velocity. Chung et al. [34, 36]. investigated the flame stabilization characteristics of non-autoignited laminar lifted jet flames of various fuels and found that the stationary lifted flame can exist only if the Schmidt number of the fuel jet is greater than unity in free jets. Many practical combustion engines such as gas turbine and diesel engines are operated under elevated pressure and temperature conditions such that they usually involve auto-ignition processes. Therefore, many studies have been performed to understand the role of auto-ignition in stabilizing lifted jet flames. Yoo et al. [37] demonstrated that auto-ignition at fuel lean mixtures plays a critical role in flame stabilization of turbulent lifted jet flames in heated co-flow.

However, such lifted flames bear the risk of lean blow out. The conventional way to address this problem is to add a pilot flame for safe operation. However, this pilot flame may generate a significant level of unwanted NO_x and add complexity to the system. The combustion concept proposed here goes a different way to ensure safe operation. Low swirl lifted flame combined with piloting of the flame by the interaction with the adjacent

flame in circumferential direction within the annular combustion chamber was adapted.

2.3.2 Swirl flames

Swirl flow is a crucial factor in the efficient operation of combustors and gas turbine engines. The physics of swirl involves a fluid motion that is accompanied by helically wound streamlines, resulting in the creation of recirculation zones that enhance flame stability, fuel and air mixing [38]. To induce swirl flow, a set of guide vanes, or swirl generators, is installed in the burner, providing a tangential velocity component to the flow. One of the most important characteristics of swirl flow is the formation of a recirculation zone due to the vortex breakdown, which results from the abrupt expansion of the swirled flow.

The Swirl number is a dimensionless quantity that characterizes the degree of swirl in a given flow field. Swirl Number is defined as the ratio of the axial flux of angular momentum $\dot{D}$ to the axial flux of the axial momentum $\dot{I}$, divided by a characteristic length. The nozzle radius R_0 is typically used as the characteristic length in the Swirl Number definition [39].

$$SN = \frac{\dot{D}}{\dot{I} \cdot R_0} \tag{2.4}$$

The effect of the swirl number significantly influences the flow structure within a combustion system. As the swirl number increases, the impact of angular momentum on the flow field increases, i.e. the tangential velocity field

exerts a greater influence on the axial velocity. Consequently, the reduction in the axial velocity due to the opposing pressure gradient becomes more pronounced. Fig. 2.8 illustrates how the swirl number affects the reduction of axial velocity along the axis. At intermediate swirl numbers, the axial velocity can even become negative, leading to a phenomenon known as "Vortex Breakdown." The recirculation effect causes hot gases to circulate between the exhaust and the reactants. Swirl flow also improves flame stabilization due to the low-velocity region at the shear layer between the inner and outer recirculation zones.

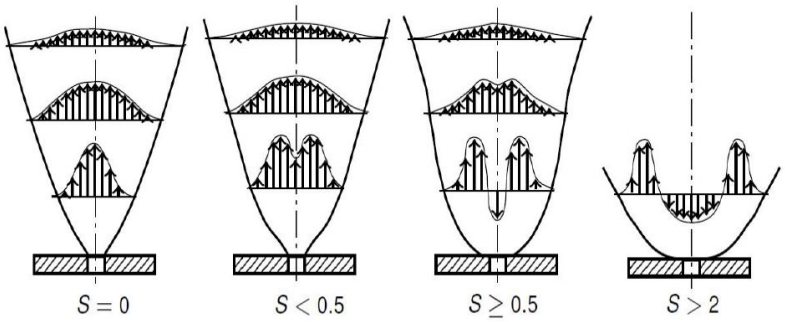

Figure 2.8: Development of the free swirl jet for different swirl numbers [40].

2.3.3 Lifted / Low-Swirl Combustion concept

This study explores the concept of a combination of low-swirl lifted flames, as proposed by Zarzalis and examined at the Engler-Buntler Institut (EBI) of the Karlsruhe Institute of Technology (KIT) [41] and investigated by Kasabov [42]. The lifted low-swirl flow structure is shown in Fig. 2.9. Previous literature has shown that a critical swirl number of 0.5-0.6 must be

exceeded to generate recirculation near the axis. However, the airblast nozzle utilized in this study has a total swirl number below the critical threshold required for strong recirculation. As a result, only a weak recirculation zone forms near the nozzle, accompanied by a region of high axial velocities that effectively push the flame away from the combustor dome, creating a reaction-free lift-off zone. The specifics of the airblast nozzle used in this investigation will be detailed further in the next chapter 3.1.3.

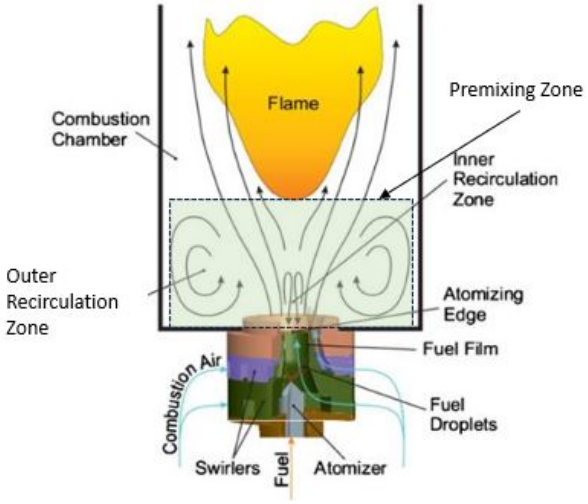

Figure 2.9: Working principle of the lifted low-swirl concept [42].

In this lifted swirl flame, the fuel and oxidizer have a certain time to mix in the premixing zone prior to the reaction zone, as illustrated in Fig. 2.9. The quality of this premixing process is influenced by various factors, including the length of the premixing zone, air velocity, and prevaporation in the case of liquid fuel. The swirl generates inner and outer recirculation zones. The inner recirculation zone (IRZ) is a central area where gases recirculate axially and is typically found close to the burner axis. The inner recirculation zone

(IRZ) in the investigated nozzle is a compact zone positioned upstream of the nozzle exit plane, where gases recirculate axially near the burner axis.

The outer recirculation zones (ORZs) generated at the edges of the burner plays a crucial role in the stabilization of the flames, primarily through enhancing the mixing by circulating hot combustion products back towards the incoming reactants. Additionally, the ORZ contributes to creating a low-velocity zone at the shear layer that is filled with hot gases, providing an ideal environment for flame stabilization.

2.3.4 Short helical combustor (SHC) concept

The inclined burners arrangement technology with burners tilted in the circumferential direction relative to the engine's rotational axis, offers several aerothermal and structural advantages over conventional combustors. This concept has been patented in different configurations by various inventors, including Hall [43], Burd [44], and Mancini [45]. The SHC is often referred to in the literature as a Short Helical Combustor due to its helical flow pattern in the chamber.

The SHC has several advantages over conventional combustors. The primary axes of all burners are tilted in the circumferential direction relative to the rotational axis of the gas turbine, creating a helical flow pattern in the combustion chamber. This helical flow pattern increases the flow residence time, allowing for a shorter axial extent of the combustor. Consequently, the length of the turbine shaft can be reduced, resulting in a more rigid core and improved shaft dynamics.

Another advantage of the SHC is that the tilted burner arrangement reduces the required deflection angle in the vane stages. This reduction in deflection angle results in a decrease in the number of Outlet Guide Vanes (OGV)) and Nozzle Guide Vanes (NGV) required and, consequently, a reduction in total pressure losses and cooling air demand.

Furthermore, the SHC's enhanced transversal exchange of heat and combustion products between adjacent flames. The SHC's helical flow pattern allows for a more efficient mixing of the fuel and air, leading to a more complete combustion process, which can result in a reduction in harmful emissions.

2.3.5 Impact of flame interaction on stabilization

The interaction between flames can be utilized to expand the stability limits. The receipt of activated compounds and heat is essential for flame stabilization [10]. One method to achieve this is to bring different flames together to allow the exchange of radicals and high temperature gases instead of recirculating the reactive flow from the flame itself, as in swirl stabilized combustion systems [11]. The concept of pilot flames in actual combustion systems is based on this principle, where a small portion of the fuel supplies a diffusion flame that operates safely far from extinction limits, providing stability to the main lean flame. However, the operation partially negates efforts to reduce NO_x emissions, as the pilot flame reaches near stoichiometric conditions, creating high temperature areas [4].

Several studies have investigated the effect of downstream interaction between two counter flow premixed flames, revealing that extinction limits are greatly altered by the mutual influence of the two flames, with different outcomes depending on the mixture composition and flow parameters [46]. Flame interaction not only influences the combustion reaction, but also the flow structure. The presence of two adjacent swirl nozzles modifies the flow field, as demonstrated by Nolan in both reactive [47] and isothermal conditions [48] through optical measurements, varying the nozzle spacing. In the non-reactive case, the differences were present but not severe, but with combustion, the axial symmetry of a single flame burner vanishes when reducing the flames distance, with significant consequences on the flame structures. Kariuki conducted a similar analysis on the effect of flame spacing, focusing on how it affects the blow-off event [49]. Flame proximity alters the blow-off process, and a difference is noted depending on the presence of the swirler. Blow-off begins first at the flame attachment point for closely spaced swirl flames, while without swirl, flame extinction begins downstream.

Transient blow-off and flame reattachment with interacting flames were studied in detail by Kwong [50] with an experimental setup similar to the test rig used in this work, consisting of a linear array of five burners at ambient pressure. Adjacent flames were found to be strongly linked, as the blow off of one flame was shortly followed by the extinction of the contiguous burner, and similarly for the reattachment process. In addition, flame interaction has proven to be helpful in partially damping thermoacoustic instabilities, as reported by Kraus in [51], investigating single and multiple burner setups with swirl-stabilized lifted flames.

2.3.6 Concluding remarks

This study introduces an innovative combustor concept for aero-engines. The unique aspect of this novel design is the integration of lean low-swirl lifted flames within the Short helical combustor arrangement. The objective of this research is to evaluate this innovative concept in terms of flame stability and emission performance, comparing it to conventional annular combustor.

Chapter 3

Experimental setup

This chapter starts with an overview of the test rig facility, detailing the setup infrastructure and specialized equipment used. It then outlines the specific operation conditions and configurations of the experimental campaign. Next, it highlights the diagnostic techniques employed, including optical and local probe methods, describing the devices, their precision, and application within the burner setup. Finally, it presents pre-investigations aimed at reducing back-flow at the exit and mimicking periodic boundary conditions.

3.1 Test rig facility

This section details the test rig facility, with a schematic drawing provided in Fig. 3.1. The central component of the experimental setup is a multi-burner array, comprising five burners that has the flexibility to be arranged either in an inline configuration or inclined at an angle (θ), as depicted in Fig. 3.2. Burner inclination is designed to mimic the helical staggered combustor configuration, where the axes of the burners are not parallel to the rotational axis of the machine. They are tilted in the circumferential direction and arranged in a helical and staggered configuration. Fuel was supplied along the burner's central axis, using a fuel feeding lance, while air supply is provided through the outer air supply tube. At the top of the multi-burner setup, an exhaust hood is positioned for the release of exhaust product gases to the external environment.

In this section, three specific subsections are introduced: the fuel path, depicted by the green lines in the schematic 3.1; the air path, distinguished by black and red lines for cold and hot air, respectively; and finally, the test section under investigation. Each of these subsections will be explained in detail.

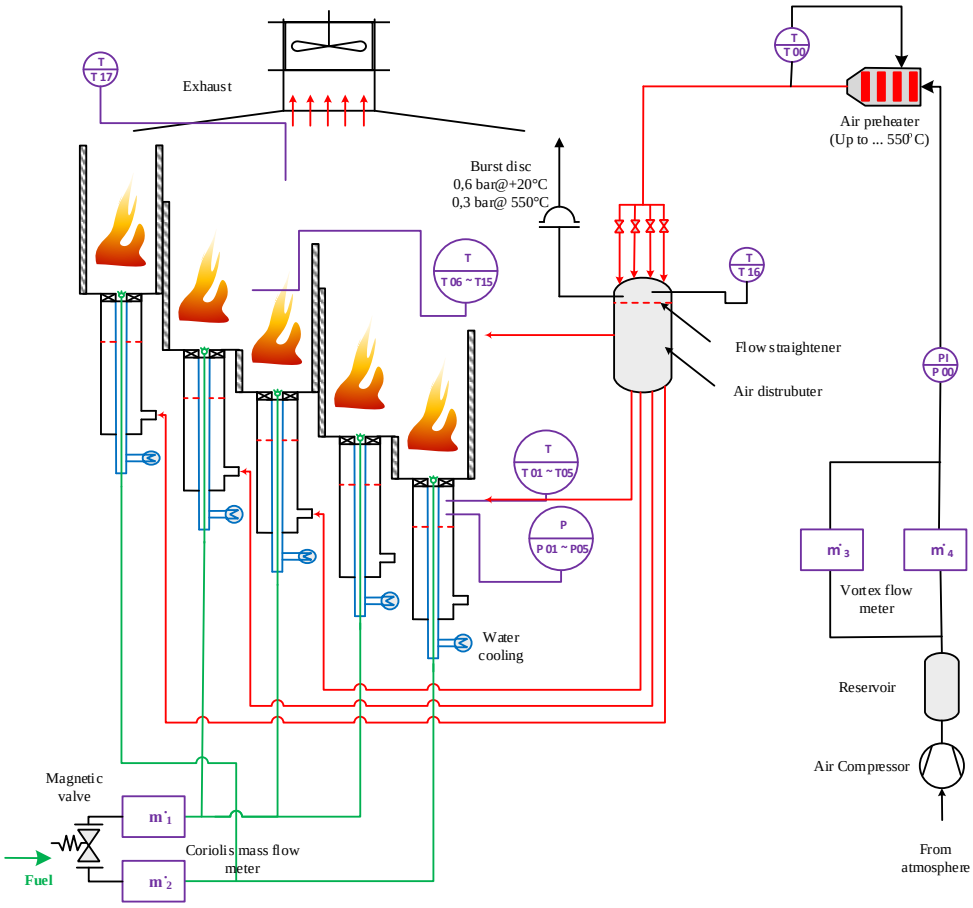

Figure 3.1: Schematic diagram of the experimental facility layout.

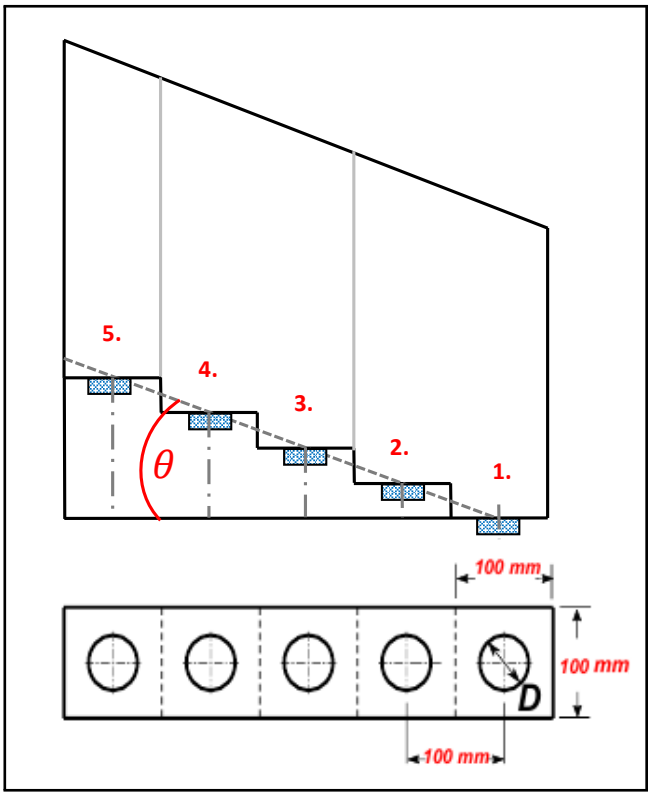

Figure 3.2: Schematic of the helical arranged combustor, side and top view.

3.1.1 Fuel feeding system

To replicate real-world aircraft engine conditions in the experiments, jet A-1 fuel was utilized. An overview of the essential physical properties of jet A-1 fuel is provided in Table 3.1, with specific focus on parameters such as density, viscosity, and surface tension, as these properties are significantly influencing the fuel atomization process. Additionally, the stoichiometric air-fuel ratio for Jet A-1 fuel was defined as AFR= 14.7, as reported by Rachner [52].

A water-cooled fuel feeding lance was employed to supply the jet A-1 fuel to the pressure swirl atomizer, reducing the risk of fuel coking at the atomizer's tip. The fuel reservoir was pressurized with nitrogen to ensure a smooth and consistent flow. As illustrated in Fig. 3.1, the main fuel supply line is divided into two paths. The first path is dedicated to supplying fuel to both the two burners on the boundaries, intentionally making them fuel-richer by 8% compared to the other burners to compensate for heat losses to the surrounding boundaries. The second line is used for delivering fuel to the

Table 3.1: Jet A-1 physical properties by Rachner [52].

Parameter		Value	Unit
Density	775 - 840	kg/m^3	
Lower heating value		43.0	MJ/kg
Dynamic viscosity		1.0	mPa.s
Surface tension		23 - 32	mN/m
Flash point		311	K
Freeze point		226	K

remaining three burners. Coriolis mass flow meters were installed on both lines, facilitating precise measurement of fuel flow rates independently for the two burners on the boundaries, as well as collectively for the remaining three. The fuel flow rate for each individual burner was regulated through the use of two distinct valves, one for coarse adjustments and the other for fine-tuning.

3.1.2 Air system

As depicted in Fig. 3.1, atmospheric air enters the system, where it is subjected to compression using a screw compressor, which can achieve a maximum flow rate of 250 g/s. After compression, the air is maintained in its pressurized state, preheated, and then expanded to near ambient pressure. This preheating process is carried out using an electric air pre-heater with a maximum capacity of 180 KW, capable of elevating the air temperature to 550°C. The airflow rate is regulated using gate control valves connected to an air distributor. Total airflow rate measurement is facilitated using a thermal flow meter. After passing through the preheating unit, atmospheric air is directed through the air distributor, which uniformly distributes air to all burner air supplies. From there, the air flows through the static airblast nozzle and enters the burner's dome. The exhaust gases generated within the combustion chamber are drawn into the test rig hood.

3.1.3 Investigated test section

The experimental investigations were conducted in a test rig comprised of multiple modular burners arranged in an array. Each individual burner featured a square cross-section base plate measuring 100 mm $\times$ 100 mm and a combustor height of 300 mm relative to each nozzle exit. The test rig operated at atmospheric pressure, and each nozzle was mounted at the center of an air supply tube with an inner diameter of 68 mm and a length of 435 mm. These air supply tubes were equipped with flow straightener plates to enhance symmetry in the air inlet velocity profiles. Combustion took place in the combined chamber of the burner array, where adjacent flames interacted freely.

A photograph of the test rig in operation with the inline burner arrangement is presented in Fig. 3.3. The combustion chamber was bordered by 2 mm thick flame fused quartz glass windows, enabling wide optical access to the interaction regions of each pair of neighboring flames. The exhaust of the combustion chamber was open to ambient air after an outlet contraction.

The burner array can be adjusted with different axial offsets to simulate various inclination angles, including 20° and 45°, as well as an inline configuration (0°). These inclinations allowed for the investigation of the impact of flame interaction offset, equivalent to the burner inclination, on combustion characteristics. Specifically, the 20° and 45° configurations represented the innovative helical combustor concept, while the inline configuration reproduced a simplified sector of conventional annular combustor, as depicted in Fig. 3.4.

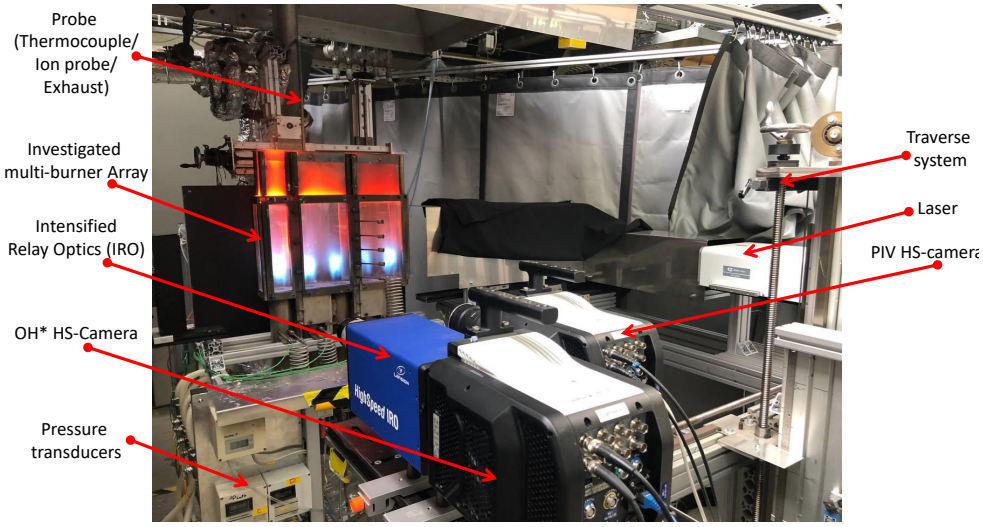

Figure 3.3: Photo of the experimental setup including an optical measurement techniques employed in the investigations.

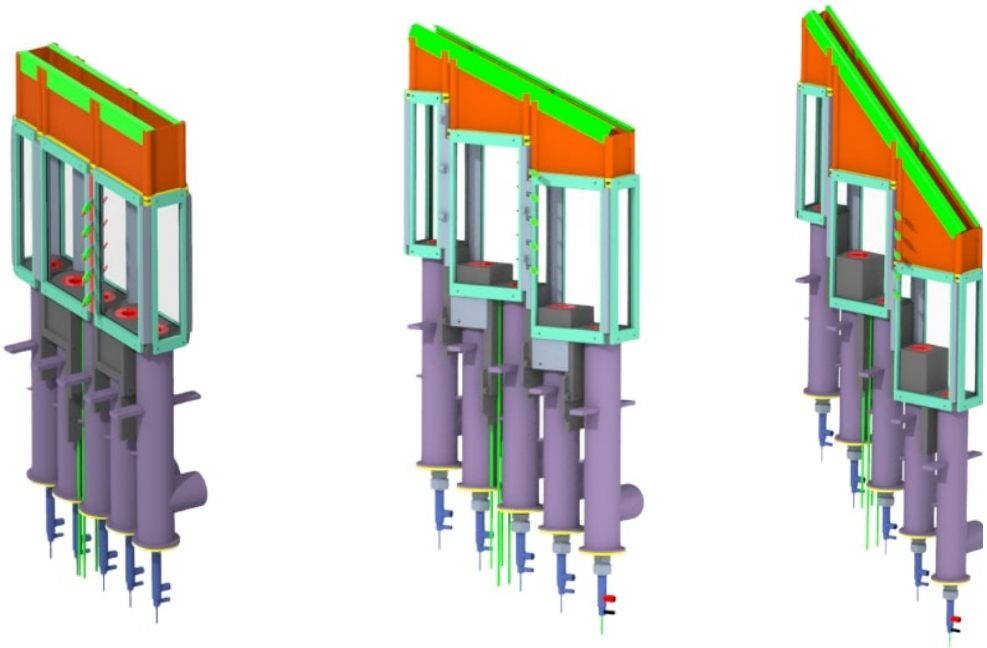

(a) Inline (θ = 0°). **(b)** Inclined (θ = 20°). **(c)** Inclined (θ = 45°).

Figure 3.4: Schematic of modular burner array at different arrangement.

Liquid fuel injection significantly influences the combustion process as the formation of combustion emissions is closely tied to the fuel atomization process and subsequent evaporation and mixing processes. Prefilming airblast atomizers, known for their fine atomization and consistent performance across various operating conditions, are commonly used in modern gas turbine engines. The atomizer utilized in this study follows the Airblast concept (see Fig. 3.5a) [41]. Swirl flow is induced by a set of guide vanes, referred to as a swirler or swirl generators, within the burner to give a tangential velocity component to the flow. The nozzle parameters are based on those used by Kasabov [53], comprising a two-swirler configuration (primary and secondary) with an outer diameter of D = 50 mm. Fig. 3.6a illustrates the nozzle components. The primary swirler consists of eight tangentially inclined vanes with an eccentricity of 10.3 mm and a passage section of 5.2 $\times$ 7.3 mm. The eccentricity determines the resulting swirl number of the air stream. The Swirl number, as defined in Chapter 2, is a dimensionless parameter representing the ratio of the axial flux of angular momentum to the axial flux of the axial momentum, divided by a characteristic length. It evaluates the strength of the primary and secondary swirlers in the airblast nozzle under investigation. The primary swirler has a swirl number of SN = 0.76, while the secondary swirler has a swirl number of zero. In comparison, the secondary swirler features twelve straight vanes with dimensions of 7.8 $\times$ 3.9 mm and zero eccentricity, providing no tangential component to the flow, and thus, no swirl. The prefilmer lip separates the primary and secondary air flows, with a final thickness of 0.35 mm, a critical parameter for atomization performance. The diffuser throat section, located at the atomization lip, allows the flow to expand before entering the combustion chamber, promoting the growth of the inner recirculation zone. Fuel atomization occurs through a

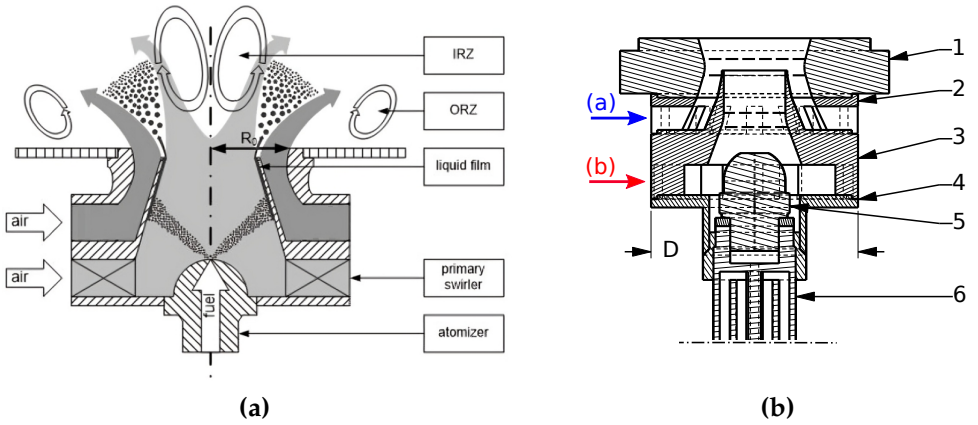

Figure 3.5: (a) Air-blast atomization process[54], (b) Scheme of the investigated nozzle type, where: (1) Diffuser, (2) Secondary Swirler, (3) Primary Swirler, (4) Inlet, (5) Atomizer, (6) Fuel Feeding Lance, (A) Secondary Air And (B) Primary Air.

two-stage mechanism. Fig. 3.5 depicts a schematic of the atomization process within the burners of the test rig. Initially, the fuel is injected via an axially located atomizer; a hollow cone atomizer with a flow number of 1.8 $\frac{kg/hr}{\sqrt{bar}}$, bore diameter of 0.35 mm, and a nominal spray inner half angle of 60°. The flow number is defined as follows:

$$FN = \frac{\dot{m}_f}{\sqrt{\Delta p_f}} \tag{3.1}$$

Smallest droplets released by the pressure atomizer don't reach the wall and are directly drawn outside of the nozzle by the primary air flow, which also pushes the thin fuel film downstream towards the atomization lip, where the final atomization is completed thanks to the shear layer that forms between primary and secondary air flows because of the different tangential velocity component. After primary breakup, droplet dimensions are further reduced

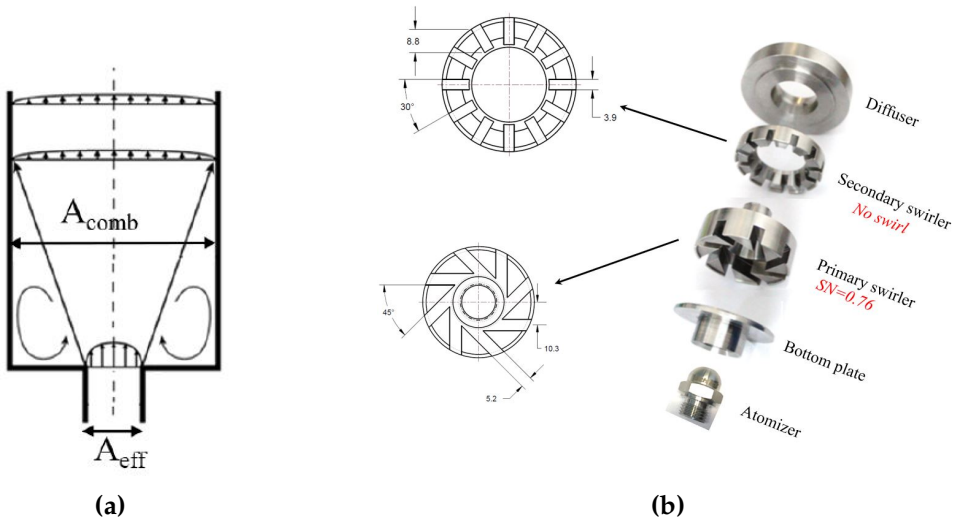

Figure 3.6: (a) Geometrical parameters for expansion ratio definition, (b) Picture of air blast nozzle parts.

by secondary breakup caused by the air flow immediately downstream of the nozzle exit.

Determining the effective area (A_{eff}) of the nozzle is crucial, as it deviates from the geometrical area due to inevitable losses. In practical applications, the effective area, a parameter directly linking mass flow rate with pressure drop across the nozzle, is employed. It represents the passage area that, ideally without losses, discharges the same mass flow as the real case with an equal pressure drop. This parameter is fundamental as it summarizes essential characteristics of the nozzle and is used to compare and scale different nozzle geometries. The effective area can be experimentally measured using the gas dynamic equations for compressible flows, as demonstrated in Equation 3.2.

$$A_{eff} = \frac{\dot{m} \cdot \sqrt{T_0} \cdot \frac{1}{p_0}}{\left(\frac{p}{p_0}\right)^{\frac{1}{k}} \cdot \sqrt{\frac{2k}{(k-1)R}} \cdot \sqrt{1 - \left(\left(\frac{p}{p_0}\right)^{\frac{k-1}{k}}\right)}} \tag{3.2}$$

$$A_{\text{eff}} = \frac{\dot{m}_{\text{real}}}{\rho \cdot u} \tag{3.3}$$

where;

$\dot{m}$ = Air mass flow rate [kg/sec]
A_{eff} = Nozzle effective area [m^2]
A_{comb} = Combustor cross section area [m^2]
p = Pressure [Pa]
T = Temperature [K]
k = Isentropic coefficient [-]
R = Gas constant [J/Kg.K]

Moreover, the expansion area ratio A_r, defined as the ratio between the combustor cross-sectional area and the nozzle effective area, plays a vital role in the creation of a recirculation zone due to vortex breakdown, which occurs as a result of sudden expansion of a swirled flow. The flow field generated by an axial or radial swirler positioned around the fuel injector has several crucial features for flame stabilization, with the primary characteristic being the formation of a recirculation zone due to vortex breakdown. In this study, the value of the expansion area ratio A_r has been selected based on the results of Kasabov [53], where a single burner with a tubular chamber was examined for different nozzle sizes, and A_r = 31.3 was chosen to achieve an expansion ratio corresponding to a real aircraft engine.

$$A_r = \frac{A_{comb}}{A_{eff}} \tag{3.4}$$

where:

A_{comb} = Combustor cross section area [m^2]

3.2 Test matrix

Several flow parameters have been examined to explore a broad spectrum of aircraft engine-like conditions. In this study, air inlet temperature, air pressure drop across the nozzle, and equivalence ratio were varied at ambient combustor pressure. Air inlet temperature plays a crucial role in the combustion process by affecting the temperature of the reactants and the reaction kinetics. The air pressure drop across the nozzle, which is determined by the nozzle geometry, influences the mass flow rate and velocity of the air entering the combustor. Finally, the equivalence ratio, defined as the ratio of the actual fuel-to-air ratio to the stoichiometric fuel-to-air ratio, is a key parameter that influences flame temperature and pollutant emissions.

During the test campaign, several combinations of these flow conditions were utilized to investigate their impacts on the combustion process in a multi-burner array. These operating conditions are presented in detail in Table 3.2. Additionally, the multi-burner array was tested at three inclination angles, namely, 0°, 20°, and 45°.

The 0° inline configuration were chosen to replicate a sector of a simplified conventional annular combustor, while the 20° and 45° configurations were designed to embody the novel helical combustor concept. By comparing the combustion characteristics of these different configurations, a comprehensive

Table 3.2: Complete test matrix of the experimental campaign.

Parameter	Value	Unit
Configuration angle	0°, 20°, 45°	
Air inlet temperature	290, 373, 473, 573, 673	K
Air pressure drop across the nozzle	1.0, 2.0, 3.0, 4.0	%
Air flow rate per burner	10.3 - 30.7	g/sec
Operating pressure	1.0	bar
Equivalence ratio	0.39 - 0.82	[-]
Power per burner	11.9 - 71.6	[kW]

understanding of the combustion process in multi-burner arrays can be obtained.

3.3 Measurement techniques

In the following section, the measurement and post-processing techniques used in this study are described. The section is divided into three subsections dealing with the applied measurement techniques. The applied invasive techniques are based on probes for temperature measurement, gas sampling, and ion current measurement. Following this, the measurement devices for air and mass flow rate are outlined. The final part of this section is dedicated to the applied optical measurement techniques, which play a crucial role in analyzing the combustion process with high spatial resolution within the combustion chamber. Three optical techniques have been employed in the investigations: OH^* chemiluminescence, Particle Image Velocimetry, and Mie-scattering.

3.3.1 Probe measurements

Over the past several years, significant advances have been made in the development of combustion diagnostics, including the use of spectroscopy and imaging, to better understand combustion processes and improve the efficiency and sustainability of combustion systems. However, while these techniques offer high levels of precision and accuracy, they can be complex, expensive, and time-consuming to implement.

In contrast, probes offer a relatively simple and cost-effective means of conducting combustion diagnostics, making them a valuable tool for advancing the understanding of combustion processes. Probes are versatile and can be used to measure various parameters, such as temperature, pressure, and species concentrations, allowing researchers to gain insight into the underlying physics of combustion.

Moreover, probes can operate in harsh combustion environments, where other diagnostic techniques may be impractical or impossible to implement. For example, probes can be used in high-temperature and pressure environments, where direct optical access is difficult or even impossible, such as in gas turbine engines and industrial furnaces. In such cases, probes can provide spatially resolved valuable data on the flow field and combustion processes, enabling the development of more efficient and sustainable combustion systems.

In addition, the use of probes can be beneficial for optimizing combustion systems, as they allow for real-time monitoring and feedback, enabling active control. This can lead to significant improvements in combustion efficiency

and reduce harmful emissions, ultimately contributing to a more sustainable energy future. In this study, three different probes have been employed including thermocouple, gas sampling, and ion probe mounted on movable 3-direction traverse system as shown in Fig. 3.7.

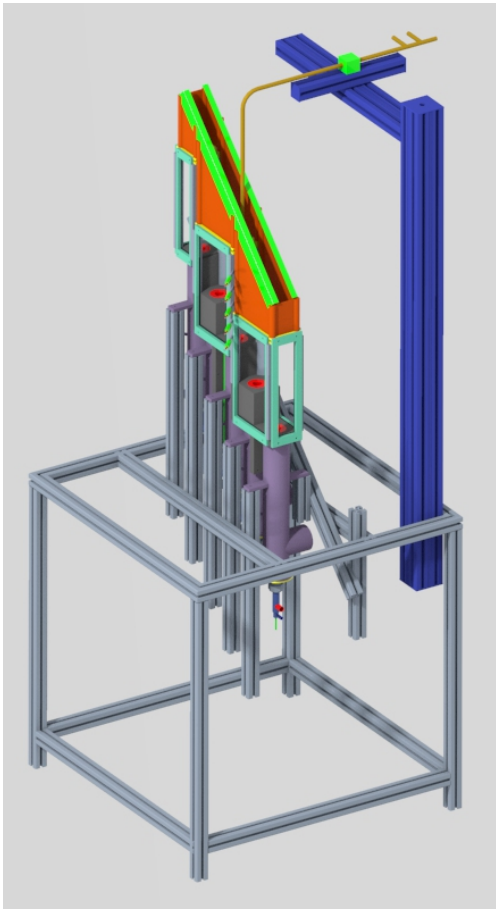

Figure 3.7: Experimental setup of the thermocouple mounted on a movable 3-direction traverse system for the test rig, allowing for precise temperature measurements in three-dimensional space.

Thermocouples

Accurate measurement of the temperature distribution of a flame is crucial for understanding the structure and stabilization mechanism of the flame. Among experimental techniques for temperature measurement in reactive environments, thermocouples stand as a cost-effective and relatively reliable choice. These devices operate on the fundamental principle known as the Seebeck effect, as elucidated by Adhikari et al. in their work [55]. In essence, the Seebeck effect manifests as the generation of electrical voltage within a circuit composed of two dissimilar electrical conductors when subjected to a temperature gradient. By quantifying this voltage, thermocouples enable the determination of the temperature difference between two points along the electrical circuit. One of these points is known to possess a specific temperature, allowing for the calculation of the absolute temperature at the measurement location. In the scope of this study, two distinct types of thermocouples were employed.

The first type comprised K-type (NiCr/Ni) thermocouples with a probe diameter of 0.5 mm and an accuracy of $\pm 1.5°C$. These thermocouples were positioned within the air plenums immediately before each nozzle. Their purpose was to measure the incoming air temperature and subsequently derive air density calculations. The second type consisted of fine-wire S-Type thermocouples, constructed from Pt10%Rh / Pt, featuring a probe diameter of 0.75 mm, a 3.5 mm ceramic sheath, and a maximum measurement range extending up to 1600°C. These S-Type thermocouples had an accuracy of $\pm 1.0°C$ without additional uncertainties related to radiation losses. They were utilized to capture the local mean temperature of the hot gases.

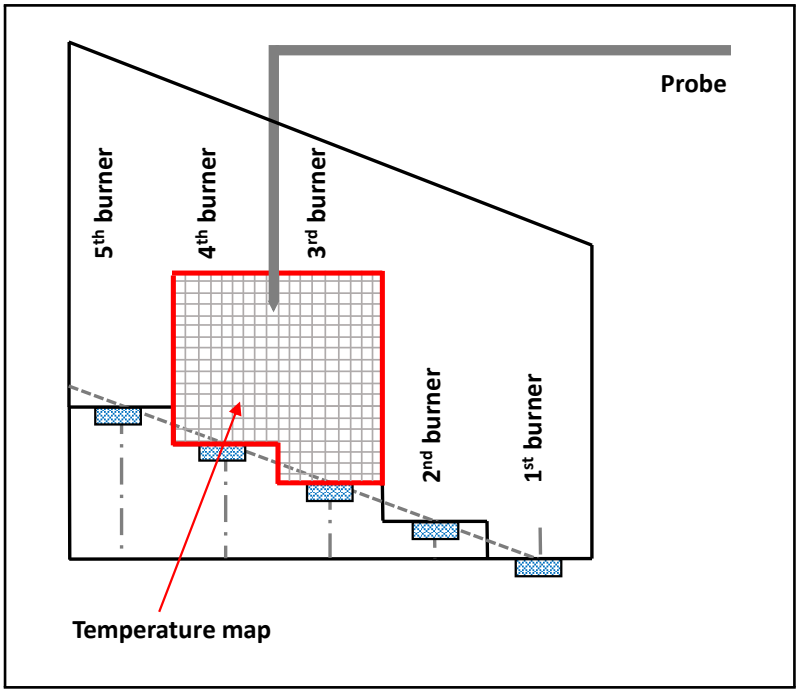

Figure 3.8: Schematic representation of the temperature map grid measured by the thermocouple, with a 10 mm spatial resolution in both horizontal and vertical directions.

The S-Type thermocouple probe was affixed to a controlled traverse mechanism, enabling precise movement along both the axial and radial directions within the combustion zone for the middle burners, as shown in Fig. 3.7. As depicted in Fig. 3.8, the thermocouple was positioned at a specific location with a measurement focus on the critical interaction region of the burners (3rd and 4th burner). The traverse system was utilized to move the thermocouple parallel to the burner array axis with a 10 mm spatial resolution in both horizontal and vertical directions. The precise control over the position of the thermocouple facilitated the acquisition of the spatially resolved temperature field, enabling an in-depth analysis of the temperature distribution

in the interaction region of the burners. In addition to the measurements within the combustion chamber, five S-Type thermocouples were positioned on the combustion chamber exit plane, as shown in Fig. 3.9. Their purpose was to capture the temperature distribution within the exhaust gases. The analog outputs from these thermocouples were transmitted to the LabVIEW program via the National Instruments NI-9213 C Series Thermocouple Input Module, where the mean temperature values were finally computed.

As an invasive measurement technique, thermocouple measurements are susceptible to errors due to their impact on the flow field and the flame. Nevertheless, the applied thermocouple type and size are considered appropriate tools for qualitative analysis of different configurations. Moreover, an assessment of radiation losses associated with the thermocouples was conducted, revealing that these losses did not notably impact the qualitative analysis between different cases.

Sample Gas Probes

The exhaust gas sampling method was employed to quantify local mean concentrations of main and trese species pollutants, including O_2, CO, CO_2, Unburned Hydrocarbons (UHC), and NO_x. To achieve this, a stainless steel water-cooled probe consisting of a central 3 mm ID tube for gas sampling was utilized, surrounded by three smaller tubes (1 mm ID) for cooling water flow. The entire probe assembly was encased within a pipe with an outer diameter of 12 mm and an inner diameter of 10 mm. the probe was mounted on a traverse system to facilitate flexible movement throughout the burner array domain.

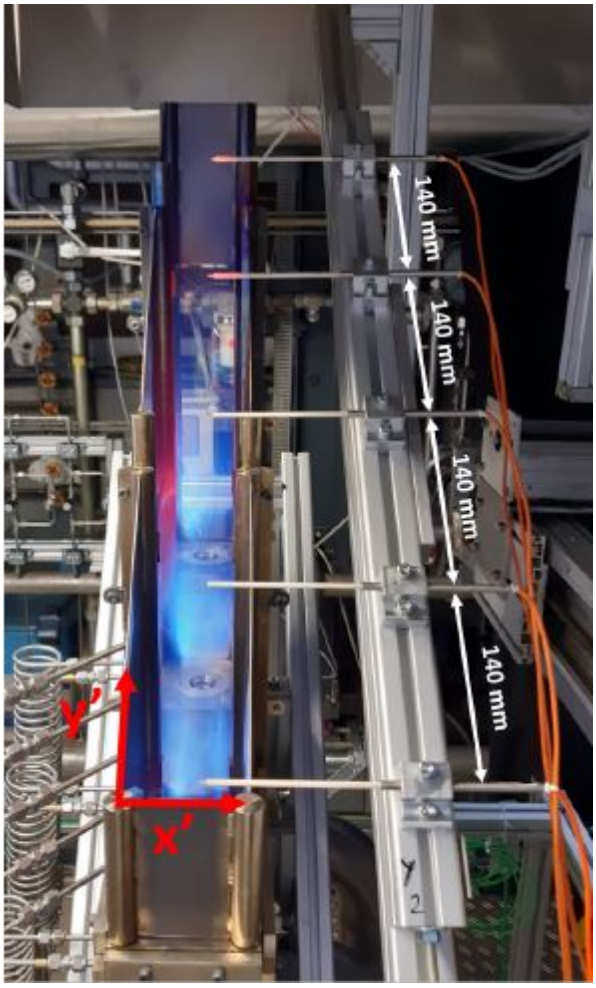

Figure 3.9: Thermocouple positioning on the outlet section in the inclined configuration.

Measurements were taken at the center of each burner outlet 10 mm before the actual exhaust point. By maintaining the probe and the transport line at elevated temperatures, the formation of water vapor condensates within the probe was prohibited.

Subsequently, the sample underwent processing by the sample gas feed unit, which filtered the sample gas, regulated its flow, and removed the water content to ensure a constant supply of clean, dry exhaust gases for each instrument. The primary analysis focused on carbon oxide measurements using nondispersive infrared gas analyzers and NO_x measurements via the UV-RAS (ultra-violet resonant absorption spectroscopy) method analyzer.

The analog outputs from these instruments were then transmitted through the National Instruments board and collected by a LabVIEW program. In this program, the signals underwent processing and were averaged over a 60-second period. In the following subsections, the measurement techniques and underlying principles of each CO and NO_x analyzer are presented.

Infrared photometer analyzer moduleUras (URAS26)

In this study, the URAS26 analyzer module, developed by ABB Ltd., operates on the non-dispersive infrared absorption principle within the wavelength range of 2.5 to 8 μm. This module was utilized for analyzing the concentrations of carbon monoxide (CO) and carbon dioxide (CO_2) in the gas sample. The device features high accuracy, typically exhibiting less than 1% of span for linearity deviation and repeatability generally below 0.5% of span, as

reported by the manufacturer. The main sources of uncertainty in concentration measurements were associated with chemical reaction quenching and aerodynamic perturbations of the flow. Chemical reaction quenching occurs when the gas molecules in the sample interact with the walls of the detector, leading to a reduction in the measured concentration. Aerodynamic perturbations of the flow can also affect the accuracy of the measurements by causing variations in the gas flow rate, pressure, and temperature.

To maintain the precision of the measurements, the URAS26 gas analyzer was calibrated prior to each measurement session. This calibration involved a zero calibration employing pure nitrogen and a span calibration employing a composition of 400 Vol-ppm CO and 10 Vol-% CO_2 in nitrogen.

Process photometer analyzer modules, (LIMAS 21)

The Limas21 UV photometer analyzer module, designed by ABB Ltd., is utilized for the accurate measurement of gas species NO and NO_2 within the ultraviolet and visible spectrum range (200 to 600 nm). Employing the UV-Resonant Absorption Spectroscopy (UV-RAS) method, this analyzer excels in measuring nitrogen oxides by comparing the absorption of light at specific wavelengths against a reference, enabling precise quantification of these gases. The device's accuracy is ensured by its low linearity deviation, typically less than 1% of the device span, and good repeatability, generally less than 0.5% of span, as specified by the manufacturer. However, accuracy may be influenced by environmental factors such as temperature and air pressure, cross-sensitivity to other gases, and the stability of the power supply. Calibration of the device involves zero-point calibration using pure

nitrogen and endpoint calibration to maintain measurement accuracy, both of which are essential for ensuring reliable and consistent performance. Additionally, the analyzer can measure both NO and NO_2, thereby providing a comprehensive analysis of nitrogen oxide levels in the emission gases.

3.3.2 Ion current probe

An extensive review of the electrical aspects of combustion was conducted by Lawton and Weinberg [56], offering a comprehensive analysis of the phenomena. The presence of positive ions was observed, with their origins primarily attributed to chemi-ionization reactions occurring within the flame as follows:

$$CH + O \rightarrow CHO^{+} + e^{-} \tag{3.5}$$

Langmuir probes emerge as the preferred technique for quantifying ion densities within flames, first introduced in the context of investigating electric discharges by Mott-Smith and Langmuir [57]. These probes are instrumental in determining the concentration of ions or electrons and typically consist of a cylindrical or spherical measurement electrode. This electrode can be subjected to either positive or negative voltage bias in relation to a reference electrode, which may be the body of the probe or even the burner itself. It is crucial that the surface area of the reference electrode substantially exceeds that of the measurement electrode to ensure that the primary current in the electrical circuit is attributed to the measurement electrode [58].

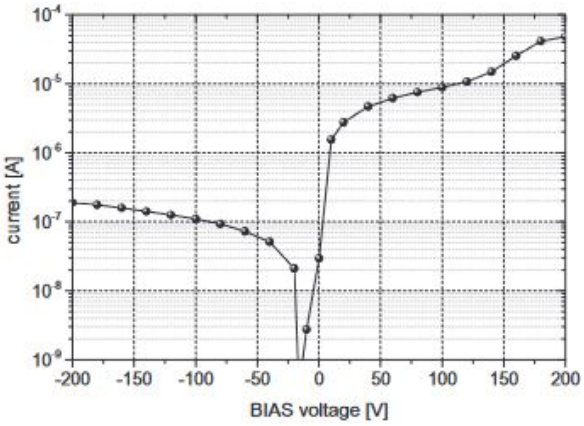

Figure 3.10: Current–voltage distribution measured inside the combustor.

The application of positive or negative bias voltage facilitates the segregation of charge carriers, allowing for the distinction between ion and electron currents. Fig. 3.10 illustrates the Langmuir potential of an ion current probe positioned within the combustor. The negative-side data are multiplied by (-1) to transform them into positive values, enabling comparable logarithmic scaling. The current for applied negative voltages is approximately two orders of magnitude smaller than that for positive voltages. Fialkov [58] provides an explanation for this phenomenon using a simplified model: Positive charge carriers primarily consist of ions, which are relatively large and slow-moving, while negative charge carriers are predominantly electrons characterized by high speed and minimal inertia. Consequently, the negative potential attracts ions and repels electrons, while the positive potential produces the opposite effect. This explanation also clarifies why the zero crossing of the current occurs at negative voltages.

Wortberg [59] investigated the relationship among heat release rate, temperature, and positive ion concentration in a methane flame. The left side of Fig. 3.11 illustrates that the heat release rate and positive ion concentration are directly correlated in the case of laminar and premixed flames. Similarly, Calcote et al. [60] conducted similar experiments with propane flames at low pressures. The findings, represented on the right side of Fig. 3.11, reveal that the highest concentrations of CH^*, OH^* and $C_2{}^*$ coincide with the peaks in positive ion concentration.

The correlation between the heat release rate and ion current signal has led to the utilization of this signal by other researchers, including Ahlheim [61], Wollgarten [54], Hoffmann [62], and Kohler [63], for flame front detection.

In this research, ion probe sensors were employed as advanced monitoring tools within the multi-burner test rig. These sensors hold potential for implementation in engines to detect conditions near Lean-Blow-Out and assess flame structures under various operating conditions.

The ion probe system components used in this investigation are illustrated in Fig. 3.12. This system comprises a water-cooled ion probe, which needs to be connected to a cooling circuit using water-glycol or oil to ensure safe operation under high-temperature combustion conditions. The ion probe is linked to a DC power supply set at a constant 150 V DC voltage throughout the experimental campaign. An isolator amplifier was used to enable accurate measurement of small current signals, and data acquisition and logging were facilitated by the MCC DT9837 Series high-precision (24-bit resolution) dynamic signal acquisition. The measurement frequency was set at 30 kHz, and data were averaged over five-minute intervals.

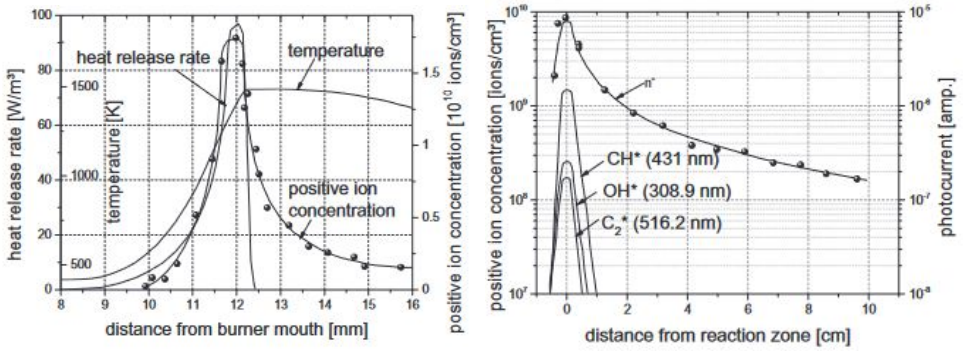

(a) **(b)**

Figure 3.11: Left: Heat release rate, positive ion concentration and temperature profile of a flat flame burner, as outlined by Wortberg [59], right: Axial distribution of CH^*, OH^* and $C_2{}^*$ and the positive ion concentration of a propane/air burner configuration at 0.05 bar and $\Phi = 0.93$.

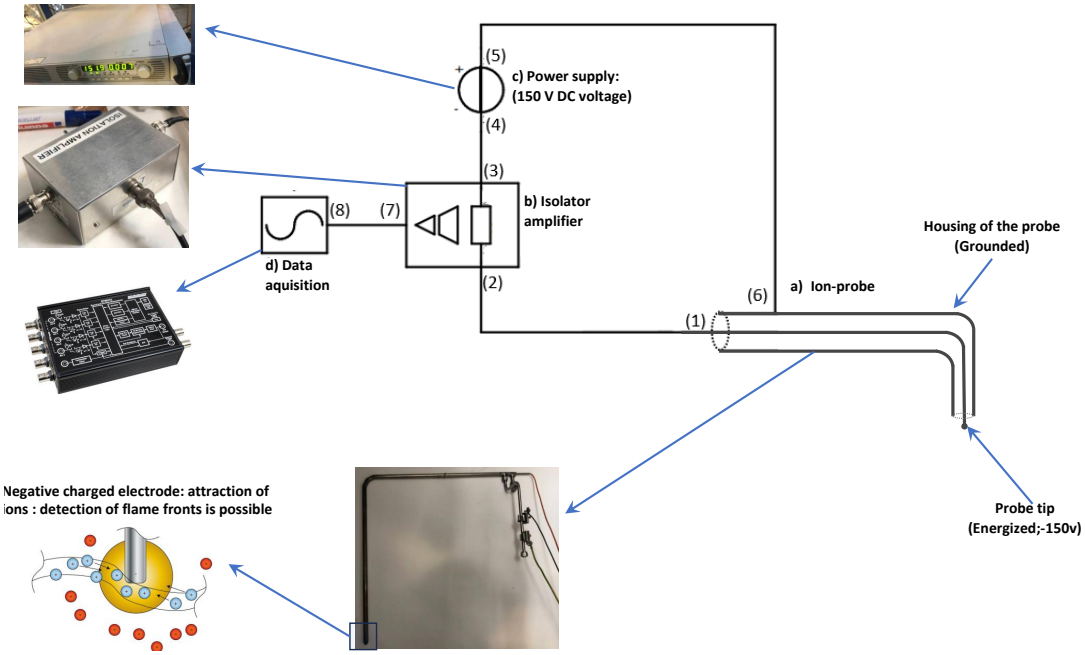

Figure 3.12: Ion probe system components.

3.3.3 Flow rate measurements

Precise measurement of the air and mass flow provided to each burner is essential for determining the experimental operating conditions, including the equivalence ratio, thermal power, and effective area.

Measurement of fuel mass flow rate

Fig. 3.13 showcases the measurement techniques used in the detailed fuel delivery system for precise data collection and analysis. In this regard, two Optimass 3000 flow meters from Krohne Messtechnik were employed to measure kerosene mass flow, with the first flow meter connected to the lowest and highest burners, and the second flow meter assigned to the middle three burners (refer to Fig. 3.1).The Optimass 3000 flow meters are Coriolis mass flow meters. The measurement unit consists of a Z-tube and two sensors. Without a mass flow, the tube vibrates with a sinus motion. When a fluid passes through the tube, the Coriolis effect causes a phase shift in the sine wave that is detected by the two sensors. This phase shift is directly proportional to the mass flow, with an accuracy of 0.1% of the measured value. Moreover, the device can measure flow rates up to 20 kg/s, making it ideal for this research applications.

In addition to the flow meters, a set of needle valves and pressure transducers were installed in each burner fuel line to control the fuel flow rate for each burner independently. The needle valves and pressure transducers operate in conjunction with the flow meters to ensure precise control and measurement of fuel flow rates. Model 8311 pressure transducer from Burkert, featuring

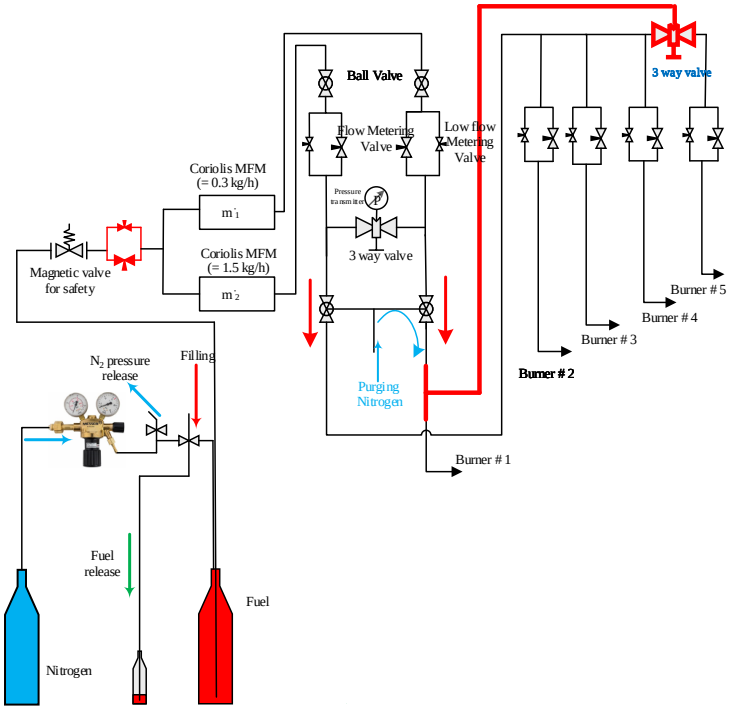

Figure 3.13: Schematic representation of the fuel line layout and measurement techniques utilized in the research study.

a ceramic cell sensor, was employed to measure the pressure in the fuel lines up to 50 bar, with an accuracy of $\pm 1.5\%$ of the full scale output. The utilization of these high precision flow meters, pressure sensors, valves and transducers, ensured accurate measurement and precise control of kerosene mass flow in the experimental setup.

Measurement of air mass flow rate

The total air flow going to the preheater was measured by thermal mass flow meter (Model F-106Cl from In Flow series of Bronkhorst). The F-106CI flow meter works in the mass flow rate range of 0 to 1000 nm^3/h refered to the normal conditions and with accuracy of $\pm$ 0.5% of full scale output.

3.3.4 OH* chemiluminescence

The heat release distribution of the flame is the most important parameter for the understanding and prediction of unstable combustion states, such as thermoacoustic instabilities, pulsed combustion, and flame propagation. The direct measurement of the spatially resolved heat release rate of flames is difficult because existing time resolved and spatially resolved measurement techniques are too complex to be applied [64]. Hence, a measurement of the intensity of light emission of the flame at particular wavelengths is used as a indicator. Chemiluminescence in flames refers to the spontaneous light emissions from chemically excited species by an electronic exchange process.

As early as in the 1970s, chemiluminescence has been identified as a potential marker for the heat release rate, reaction zone, and equivalence ratio. The major species are formed in the thin reaction zone thereby their detection can provide information on the location of reaction zone [65]. The generation of chemiluminescence mainly includes two steps: the formation (R1) and the radiative transition (R2) of excited-state radicals:

$$A + B \longrightarrow R^* + \text{others} \qquad \text{(R1)}$$

$$R^* \longrightarrow R + h\nu \quad \text{(R2)}$$

$$R^* + M \longrightarrow R + M \quad \text{(R3)}$$

where A, B, and R are different ground-state radicals; R^* is an excited-state radical; and M is a third body species. It is important to highlight that not all excited-state radicals are involved in the process of generating chemiluminescence. As shown in reaction R3, some of them collide or react with other species [66]. In hydrocarbon flames the four major emitters found are OH*, CH*, C2*, and CO2* [67]. The flame spectra in the visible and ultra-violet (UV) regions occur generally due to the transition of electrons in molecules from the excited configuration to the ground state. A typical flame spectrum obtained from hydrocarbon combustion is shown in Fig. 3.14.

Among all the chemiluminescent species OH* is commonly used in experimental investigations as representative for flame heat release which gives a strong light emission with peak intensity at about 309 nm. in this regard

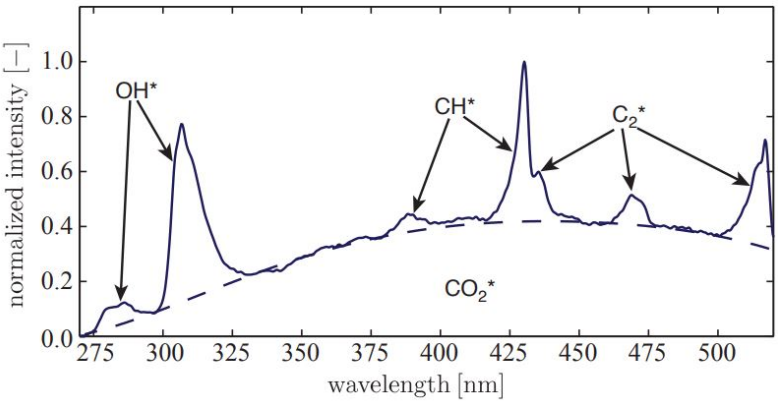

Figure 3.14: Chemiluminescence spectrum of a stoichiometric premixed methane-air flame. [68].

OH* was used in the present study to evaluate the reaction zone shape and position of the flame.

The electronically excited OH* radical is known to be generated via various pathways, with the primary formation reactions being:

$$CH + O_2 \longrightarrow OH^* + CO \tag{3.6}$$

$$CHO + O \longrightarrow OH^* + CO \tag{3.7}$$

$$H + O + M \longrightarrow OH^* + M \tag{3.8}$$

Here, M is defined as a third body and represents an inert concision partner not participating in the reaction bonds. Among these reactions, 3.6 is the main formation mechanism of OH* in hydrocarbon combustion [65]. Upon reaching an electronically activated state, the OH* radical can return to its stable ground state, OH, through two possible mechanisms: fluorescence or collisional quenching. The corresponding reactions are as follows:

$$OH^* \longrightarrow OH + \frac{hc}{\lambda} \tag{3.9}$$

$$OH^* + M \longrightarrow OH + M \tag{3.10}$$

Fluorescence (reaction 3.9) involves the spontaneous emission of a photon, which carries the energy difference between the two energetic states [10], represented by the term $\frac{hc}{\lambda}$, where c is the speed of light, λ is the wavelength of the electromagnetic radiation, and h is the Planck constant. Fluorescence does not occur between any energetic levels, but only certain transitions can lead to photon emission. Collision with a third body (reaction 3.10) can

lead to both higher and lower energetic levels, changing the vibrational or rotational state. The equilibrium distribution depends on the ratio between upward and downward transitions, which is a function of temperature. Equilibrium distribution of excited radicals, together with Einstein coefficients for spontaneous emission, determines the emission spectrum [68].

The Einstein coefficients for spontaneous emissions represent the proportionality factor between the number of electronically excited radicals and the chemiluminescence intensity, as they quantify the probability of light absorption or emission by a molecule. The chemiluminescent emissions of OH^* originate from a transition to the ground state, typically written as $X^2\Pi_i$ from the electronically excited state denoted as $A^2\Sigma^+$ [69]. Various vibrational and rotational levels are present in these energetic states, contributing to the chemiluminescence band. The intensity peak near 309 nm, shown in Fig. 3.14, originates from the transition $X^2\Pi_i\,(v'' = 0) \longrightarrow A^2\Sigma^+\,(v' = 0)$ [68].

Besides the origin of OH^* chemiluminescence, it is important to understand how it can be used in experimental analysis to characterize the flame behaviour. This aspect has been investigated from different perspectives in previous works. Najm et al. [70] studying the reaction mechanism of methane combustion discovered that only a small percentage of carbon atoms is involved in the reactions that lead to the formation of chemiluminescent species OH^*, CH^* and C_2, concluding that they can not be used for marking the turbulent flame front or heat release. The integral visible chemiluminescence emission was measured in a turbulent swirled premixed flame by Lee and Santavicca [71], reporting a dependency from the fuel flow rate and global equivalence ratio, but also from aerodynamic flame stretch and curvature

and premixing level. Hardalupas and Orain [72] correlated OH^*, CH^* and CO_2^* chemiluminescence emission to the spatially resolved heat release rate in low Reynolds counter flow premixed flames. The high Reynolds range was studied by Ayoola [73], who concluded that OH^* can not be used to represent local heat release in turbulent flames, because of its sensitivity to strain and turbulence. Lauer came to the same conclusion for flames with mixture gradients, while for premixed flames with a correction to consider the effects of the flame strain rate and another one to eliminate the broadband CO_2^* emission, OH^* is considered representative for local heat release [68].

According to the study results, the OH^* chemiluminescence measurements presented here do not offer a spatially resolved distribution of flame heat release or any specific quantity. However, they qualitatively visualize flame conditions and identify the main reaction zone. In addition to the above considerations, it has to be remembered that chemiluminescence is a line-of-sight technique, meaning that the emission intensity detected by the instrument includes chemiluminescence contributions integrated along the line that connects the sensor to the measured point. Usually in time-averaged measurements the intensity on the flame mid plane is reconstructed assuming axial-symmetry with deconvolution methods as the inverse Abel transform. In the present study, although rotational symmetry is not necessarily present in a combustor with a rectangular burner configuration, it is assumed to exist in the core flame region. Consequently, an inverse Abel transform has been attempted, which will be described later.

In this work, the OH* chemiluminescence emission was detected using an intensified camera equipped with a UV lens and UV band pass filter. The Lavision Phantom V1212 camera, coupled with the HighSpeed IRO image

intensifier device, was utilized to achieve high sensitivity and accuracy in the detection of OH* emission. The camera was set to 5 kHz recording frequency, with a 1280 x 800 pixel resolution. The image intensifier had a spectral range of 190-800 nm and a minimum exposure time of 100 ns, with a maximum repetition rate of 2 MHz. The Lavision UV focusing lens, with a focal length of 85 mm and optimized wavelength in the UV spectrum (220-450 nm), was used to ensure high light collection efficiency. A UV band pass filter was applied to the lens to capture only the OH* chemiluminescence peak emission, of a center wavelength of 309 nm. 1000 image were recorded with the Lavision DaVis software version 10. After recording, a background light intensity subtraction was used to reduce the noise and then averaged.

The camera used for the OH* chemiluminescence images captures a line of sight integration of the OH* chemiluminescence of the flame. In order to recover the radial distribution of the OH* chemiluminescence from the projection, Abel deconvolution schemes [74] were applied. Rotational symmetries have to be assumed for the application of this technique.

3.3.5 Particle Image Velocimetry (PIV)

Particle Image Velocimetry (PIV) is an optical technique for determining spatially resolved velocity fields based on the well known equation:

$$\text{Speed} = \frac{\text{Distance}}{\text{Time}} \tag{3.11}$$

In PIV small light scattering particles (seeding particles) are added to the flow. A short, double-pulse laser beam is formed into a light sheet illuminating

these seeding particles at the measurement plane twice within a short time interval Δt. In 2D-PIV, employed in this investigations, the trajectory of the particles, which follow the flow, can be captured by the scattered light of these particles and recorded onto two consecutive frames of a high resolution digital camera. The camera images are divided into rectangular regions called interrogation windows shown in Fig. 3.15. For each interrogation window, the area from the first and the second laser pulse/camera frame are cross-corrected to produce an ensemble average particle displacement vector. Doing this for all interrogation windows produce a vector map of average particle displacements. Using the image analysis techniques illustrated in scheme 3.16, the instantaneous velocity vector fields with high spatial and temporal resolution are obtained. In this work, two-dimensional PIV measurements

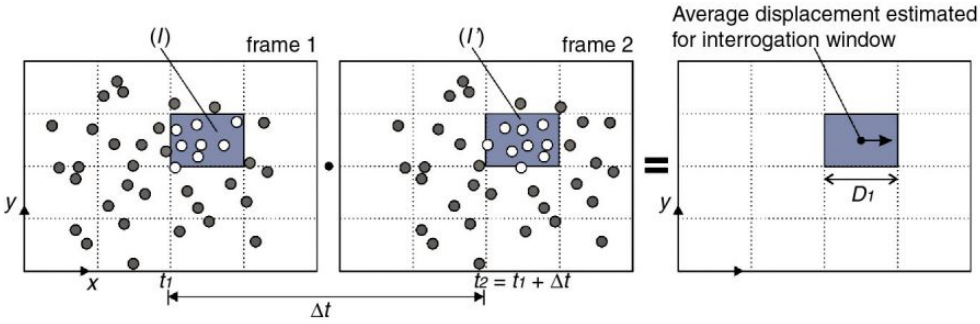

Figure 3.15: Schematic illustrating how the image frames are subdivided into interrogation windows [75]

were performed using a diode-pumped, dual cavity, high-speed Nd:YLF laser (Litron LD25-527 LM2827) together with a high-speed camera (Phantom V1212, resolution 1280x800 pixels) set to 5 kHz recording frequency (double frames at maximum resolution). 1000 double frame images were recorded per measurement for total measurement time of 200 ms and the time separation

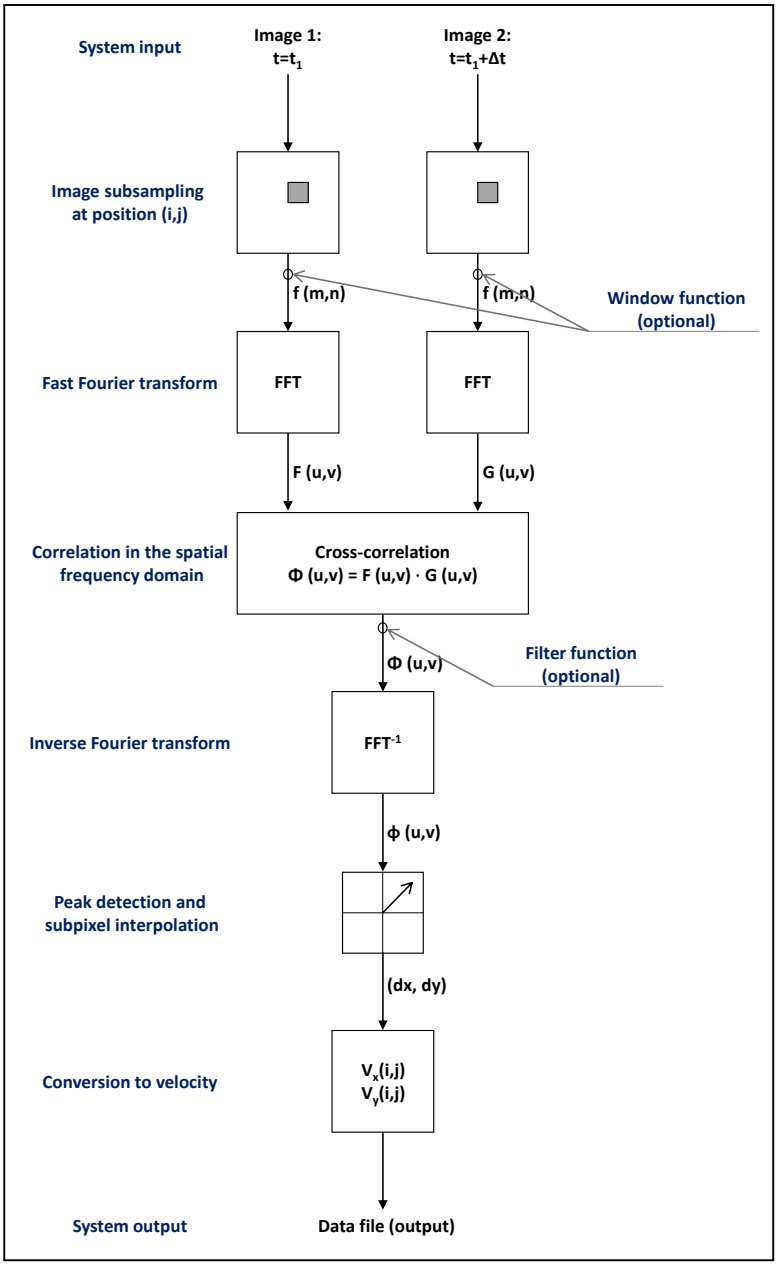

Figure 3.16: Numerical post processing flowchart of PIV, reproduced from [76]

between the laser pulses was set to 20 μs. The camera was calibrated and focused using a rectangular target with 5mm dot spacing centered at the fuel nozzle.

For non reactive flow investigations, silicone oil was seeded into the air flow using aerosol generator (Palas AGK 2000) with a particle size of 0.5μm. For non reactive flow investigations, Aluminum oxide (Al_2O_3) with a particle size of 1 μm was used as seeding material and was fed into the air flows for each burner by using fluidized bed seeders. The Aluminum oxide seeding particles were dried overnight prior to each measurement. A 532/10 nm band-pass optical filter was used to filter the background light. The field of view (FOV) for the PIV measurements was focused on the two central burners. Depending on the height of the laser light sheet (100 mm) and the resolution of the camera, the FOV was divided into two axial parts (PIV #1 and PIV #2) in Fig. 3.17. Velocity field calculations were performed using a commercial PIV software (DaVis 10.2, LaVision). Pictures were pre-processed by subtracting the background illumination and masking off all reflection zones near to the burners domes. Cross correlation started at 48px window size and 50% overlap decreasing to 32px window size and 50% overlap is adjusted.

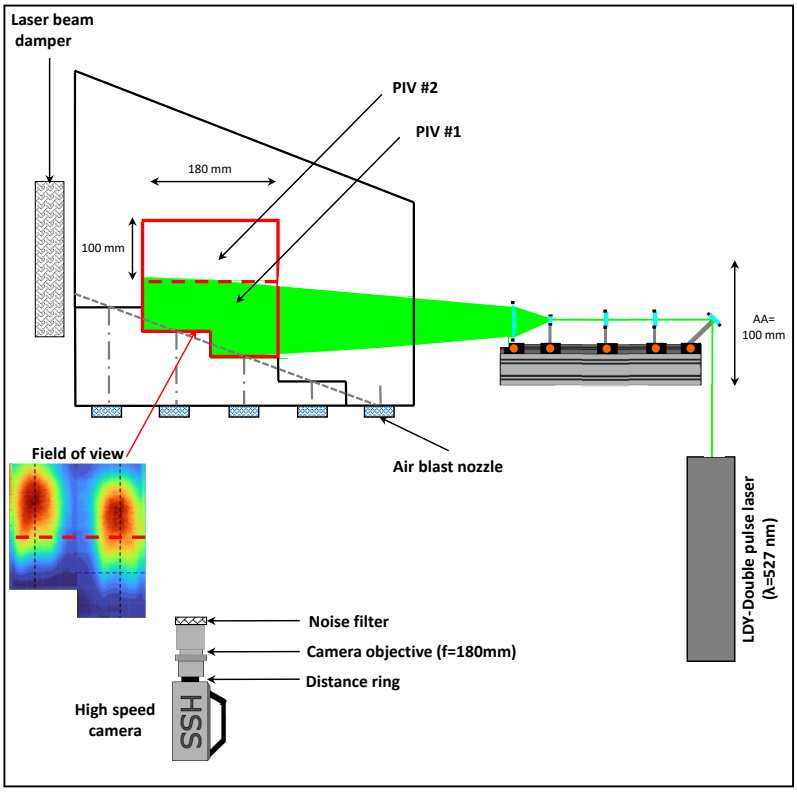

Figure 3.17: Schematic depicting the 2D PIV arrangement and the laser sheet.

3.3.6 Mie scattering

The Mie scattering laser diagnostic technique was employed to qualitatively analyze spray characteristics, which in turn provides insights into flame characteristics. This includes crucial parameters such as the penetration depth of the fuel spray into the flame and the hollow cone angle of the spray. The experimental setup for Mie scattering employed the same configuration as the Particle Image Velocimetry (PIV), utilizing identical components, including a laser with a wavelength (λ) of 532 nm, optical elements, a high-speed camera, and a filter. Seeding particles were not applied, as the scattered light from the fuel droplets was collected.

3.4 Preliminary Study: Flow deflection and boundary condition challenges in SHC

The implementation of Short Helical Combustors (SHC) in practical engines has been challenging, despite their potential advantages, such as compactness and a reduced number of nozzle guide vanes (NGVs). A significant issue is the reduction in the nominal deflection angle of the flow within the combustor, caused by the interaction of swirling flows from adjacent flames. To understand this flow deflection in the inclined case, the no-deflection scenario relative to the machine axis in the context of an inline configuration or sector from a conventional annular combustor was examined, as shown in Fig. 3.18. In an annular combustor, the flame axes are parallel to the machine axis, which leads to favorable boundary conditions for the investigated sector. In contrast, the inclined case exhibits undesired flow deflection, as depicted in

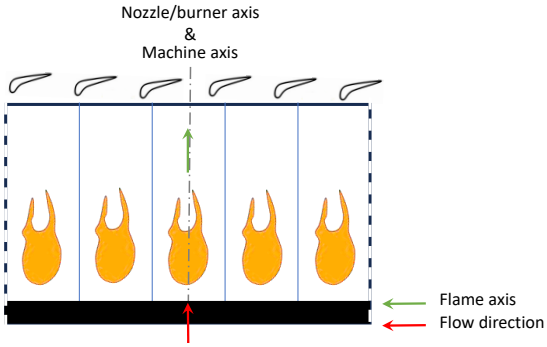

Figure 3.18: Schematic diagram illustrating the flow and flame directions in the inline configuration.

Fig. 3.19. This phenomenon, associated with high swirl flows, was identified and explained by Ariatabar et al. [33]. Such deflection of the flow back towards the machine axis can significantly reduce the benefits of the SHC concept. Utilizing low swirl flows may help mitigate these shortcomings by directing the flow more favorably towards the NGVs. This approach can reduce the required number of NGVs, decrease cooling demands, and result in a lighter weight aero-engine.

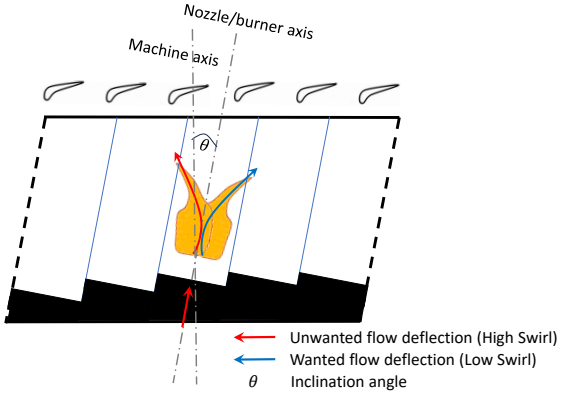

Figure 3.19: Schematic diagram illustrating the flow and flame directions in high and low swirl cases within the inclined annular configuration.

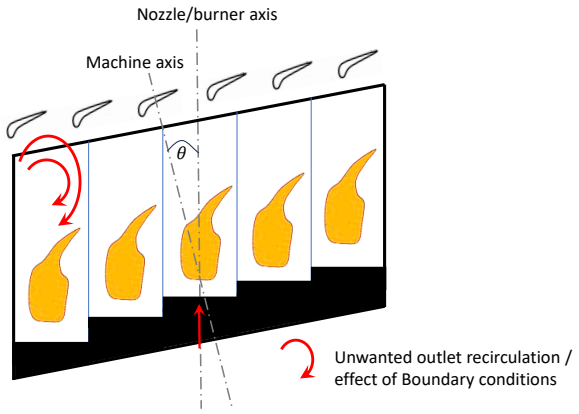

Figure 3.20: Schematic diagram illustrating the effect of boundaries in burner array with 5 burners, layout rotated in the test case to avoid buoyancy impact.

In this testing campaign, early experiments revealed that using the SHC with low swirl flow in a model combustor with a 5-burner array results in favorable flow deflection towards the NGVs. This flow deflection can be attributed to an asymmetric pressure field near the sidewalls of the staggered dome, induced by the Coandă effect, as elaborated by Hoffmann in a numerical study [77]. This undesired behavior at the exit is expected with a finite number of burners due to boundary wall effects but is not anticipated in a real annular engine. In the burner array under investigation, this flow deflection phenomenon creates a substantial backflow vortex at the outlet of the lower burner sectors, as depicted in Fig. 3.20. The backflow introduces cold ambient air into the combustor, altering the global air-fuel ratio and leading to unrealistic operating conditions. These observations highlight the need to explore different outlet configurations to address and mitigate backflow issues.

To address the aforementioned issue of boundary conditions, two outlet configurations have been investigated. The first configuration features an open exhaust outlet as shown in Fig. 3.21a, while the second configuration involves the implementation of an outlet contraction, as shown in Fig. 3.21b. A comparison of these configurations is provided in Fig. 3.22, which illustrates the temperature fields at the outlets. Temperature measurements were taken using five S-type thermocouples arranged in a grid with a cell length of 1 cm, moving in both the parallel (y-direction) and perpendicular (x-direction) dimensions.

As shown in Fig. 3.22, the open outlet configuration results in a non-uniform temperature distribution due to cold air recirculation from the lower burners and heat accumulation at the higher burner. In contrast, the outlet contraction configuration (Fig. 3.21b) significantly reduces the recirculation zone, leading to a more uniform temperature distribution at the burner array exit. However, there is still a slight cooling effect in the lower burner and heat accumulation in the higher burner. The contracted outlet significantly improves the temperature distribution qualitatively, making it clear that the central burner is not affected.

Therefore, the outlet contraction configuration (b) was selected for further detailed studies due to its improved applicability for future applications and its independence from prior knowledge of outlet flow angles.

(a) Open outlet. **(b)** Conteracted outlet.

Figure 3.21: Various outlet configurations applied to the test array.

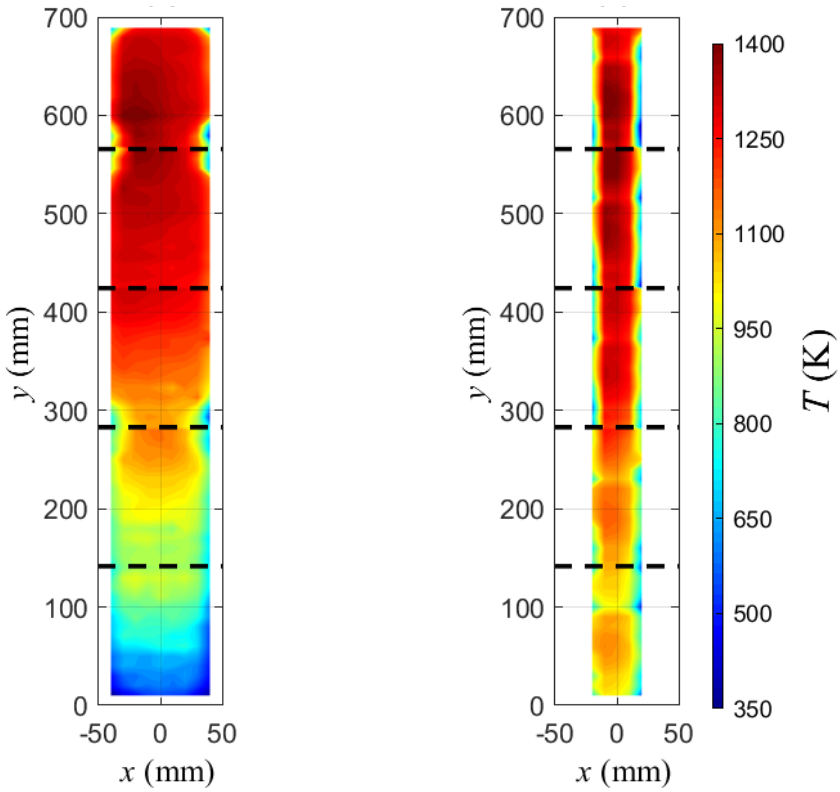

(a) Open outlet. **(b)** Conteracted outlet.

Figure 3.22: Visualizing the impact of outlet configurations on the temperature field for 45° inclined burners at 3 % pressure drop and 0.47 equivalence ratio: (a) Open Outlet, (b) Partially Blocked Outlet, and (c) Contracted Outlet. The dashed line represents the edge of each individual burner.

Chapter 4

Results and discussions

The current study investigates the impact of burner arrangements, specifically inclination angles, on the stabilization mechanism, flame structure, and emissions of kerosene/air flames in a multi-burner setup using lifted low swirl flames under lean conditions. The results begin with an investigation of the Lean Blowout (LBO) limits and the flame stabilization mechanism of this innovative concept across a wide range of operating conditions and compare the results with inline configurations under the same conditions (see Section 4.1).

Section 4.2 elucidates the flame structure and lift-off height under various operating conditions, including changes in air inlet temperature and air mass flow rate defined by air pressure drop across the nozzle, for both inline and inclined configurations.

Section 4.3 analyzes burner emission performance under different conditions, providing insights into how burner arrangements influence emissions, focusing particularly on NO_x and CO levels.

Lastly, Section 4.4 details the use of ion-probe techniques for monitoring the conditions near to the LBO and flame structure.

4.1 Lean blowout limits of the CHAIRLIFT concept

The stability range of a combustor is essential for safe engine operation and directly impacts pollutant emissions. A wide stability range allows the combustor to operate at low combustion temperatures without relying on pilot flames or nozzle staging, resulting in very low NO_x emissions across various cycle conditions from idle to takeoff. Idle conditions require very lean combustion with low inlet temperatures to maintain stability and efficiency at low power settings. Conversely, takeoff conditions demand a rich fuel mixture and high fuel flow through the main injectors to provide the necessary power and thrust. This wide range of operating conditions ensures that the burner can efficiently handle the varying demands of different flight phases, from idle to full power takeoff.

Flame blowout occurs when the flame inside a combustor is extinguished as a result of e.g. local extinction due to high instantaneous strain rate. Thus, understanding and controlling the stability range of the combustor is crucial

for the safe and efficient operation of the engine, as well as for reducing pollutant emissions [78].

In this research, the lean blowout (LBO) limit is defined as the lowest possible fuel amount before extinction or blowout occurs while keeping the airflow constant. The LBO measurements helps in obtaining the minimum fuel flow rate for a particular engine conditions below which the flame cannot sustain itself. The LBO measurements are performed starting from stable conditions, that is maintained for a sufficient time, the air flow rate is kept fixed while the fuel flow rate is lowered slowly in steps until the central flame is extinguished. To prevent premature blowout of side burners resulting from heat loss, those side burners were operated 8% more fuel rich, which resulted in the middle burner extinguishing first.

4.1.1 Impact of the air inlet temperature

Fig. 4.1 illustrates the effect of air inlet temperature (T_{Air}) on the flame stability limits of low-swirl, turbulent non-premixed Jet A1-air flames at different tilt angles. In this figure, The air number, λ, is a dimensionless parameter that describes the ratio of the actual air-to-fuel ratio to the stoichiometric air-to-fuel ratio. λ_{LBO} is the maximum air number where the stable conditions are achieved before the blow-out conditions. It can be noted that at low air inlet temperature ($\approx$ 290 K) the flames have a very good stability performance for all burners alignments and pressure drops. The measurements of the fuel spray (as depicted in Fig. 4.7) show that under these low temperature conditions fewer droplets pre-evaporate upstream near the burner dome and large droplets move outward due to centrifugal force causing localized enrichment

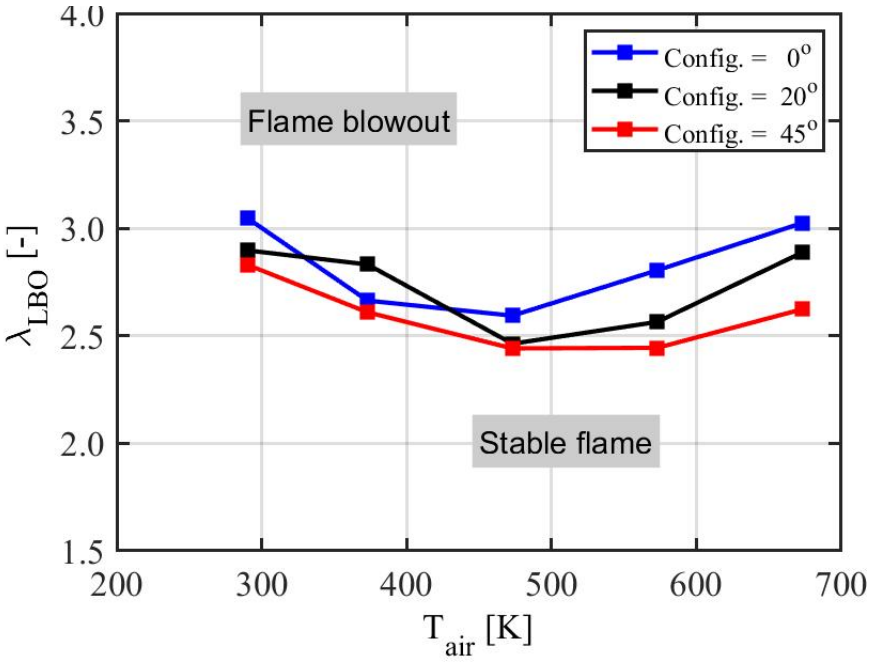

Figure 4.1: Impact of air inlet temperature on lean blow out characterized by air number at pressure drop across the nozzle of 3% for different burner array arrangement at low swirl number, SN=0.47.

in the shear layer zone near to the outer recirculation zone (ORZ) where the flame stabilizes.

By increasing the air inlet temperature to 473 K and maintaining a constant air pressure drop of 3% across the nozzle (constant mass flow rate), the fuel evaporation time decreases. This results in better mixing and a higher degree of premixing and pre-evaporation. This can be observed in Fig. 4.7, which shows that the fuel spray and reaction zone are well separated. In consequence, most of the droplets evaporate more near to the nozzle axis and more far away from the ORZ which reduces the flame stability but it is very promising behavior regarding emission performance.

Further increasing the inlet air temperature to the highest investigated level ($\approx$ 673 K) at the same air pressure drop, increases the flame stability due to the increase in the flame speed compared to the increase of the flow velocity which could be explained by the premixing theory [79]. According to the premixing theory, lifted flames stabilize in a turbulent regime where the stoichiometry is dictated by the balance between the local gas flow velocity U_{gas} and the turbulent burning velocity S_T at the flame stabilization point. The velocity of the jet stream leaving the nozzle obeys the gas-dynamic equation and changes with the air inlet temperature as ($U_{gas} \propto \sqrt{T_{gas}}$) at constant pressure drop. Due to the square-root dependency, the increase in the jet exit velocity with the temperature is more pronounced at lower temperatures and flattens out at higher temperatures. However, the laminar burning velocity has a quadratic dependence ($S_L \propto {T_{Air}}^2$). Thus, the increase in burning velocity is greater than the increase in inflow speed shifting the location of the reaction zone upstream and enhances the flame stability. An additional factor that plays a role in flame stabilization of such low swirl flame is the size of the outer recirculation zone as described by Kasabov et al. [42]. From the flow field measurements inside the middle burners at different air inlet temperatures, the size of the back-flow in the outer recirculation zone is estimated in Fig. 4.6 by calculating the area bounded by the zero axial velocity line which used as an indication of the size of ORZ. As we can see, size of the outer recirculation zone, measured in 2D plane, increases linearly with air inlet temperature, pushing the low velocity shear layer towards the nozzle axis where the flame stabilizes.

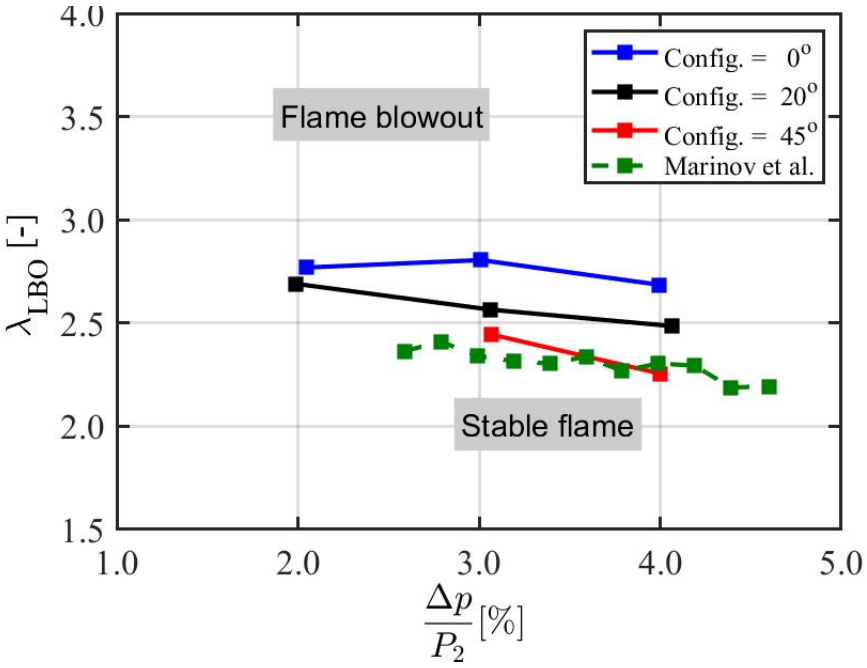

Figure 4.2: Impact of air pressure drop across the nozzle on lean blow out characterized by air number at air inlet temperature of 473K for different burner array arrangement at low swirl number, SN=0.47 compared to previous investigation of single burner at higher swirl number, SN=0.76 by [80].

4.1.2 Impact of the inclination angle (different offsets)

The particular focus of this research is to study the influence of the tilt angle on the flame stabilization limits and stabilization mechanism to evaluate this innovative helical-arranged burner array and compare it to the inline arrangement as a representative of the conventional annular combustor at different operating conditions. Fig. 4.2 shows a good stability range of lifted flames despite the high degree of premixing (similar or even better lean-blow-out compared to typical moderate swirl stabilized flames with big inner recirculation zone for lean injection systems investigated by Marinov et al.

[80]). Fig. 4.1 compares the lean stability limits for two different tilt angles, 20° (solid black line) and 45° (solid red line), with the inline arrangement at 0° (solid blue line) at different air inlet temperature. The figure indicates that the flame stability margins for all investigated configurations exhibit a similar trend as the air inlet temperature increases, with different magnitudes. The interesting observation here is that the flame stability at low air inlet temperatures (near the idle engine conditions) is controlled by the slower evaporation of the fuel droplets creating locally rich pockets near the flame root as explained in the previous section 4.1.1 and with a little impact of the alignment of the burner. At high air inlet temperatures, the blow-off limit of the inline case is surprisingly higher than with inclined arrangements. The present results reveal that the blow-off limit is decreasing with increasing the tilt angle at higher air inlet temperatures. PIV and temperature measurements were performed in order to characterize the reacting flow field and hence help the understanding of the aforementioned flame features/observations. It is clear that in Figs. 4.3 and 4.7, under all conditions of the inline arrangement, the flow field structure is dominated by the ORZ at the sides of each individual burner. The size and location of these ORZs are dependent on the ratio of air inlet temperature to adiabatic flame temperature (T_{Air}/T_{ad}) which determines the flow expansion inside the combustor. The recirculation zones cause low-velocity regions where the flame can anchor. Additionally, it acts as a radical pool and thermal reservoir which helps the heat transfer from the flame to the fresh mixture upstream of the lifted flame base, and the resulting flame speed is increased, as well as increasing the level of turbulence which helps the flame to stabilize. The size and the temperature of the outer recirculation zone are very important parameters in the stabilization of this lifted low swirl flame consistent with the previous investigations of

Kasabov et al. [42]. The estimated size of ORZ shown in Fig. 4.6 shows that the stabilization of the inline case is enhanced at elevated T_{Air} due to the significantly larger ORZ. The measured temperature profiles in a

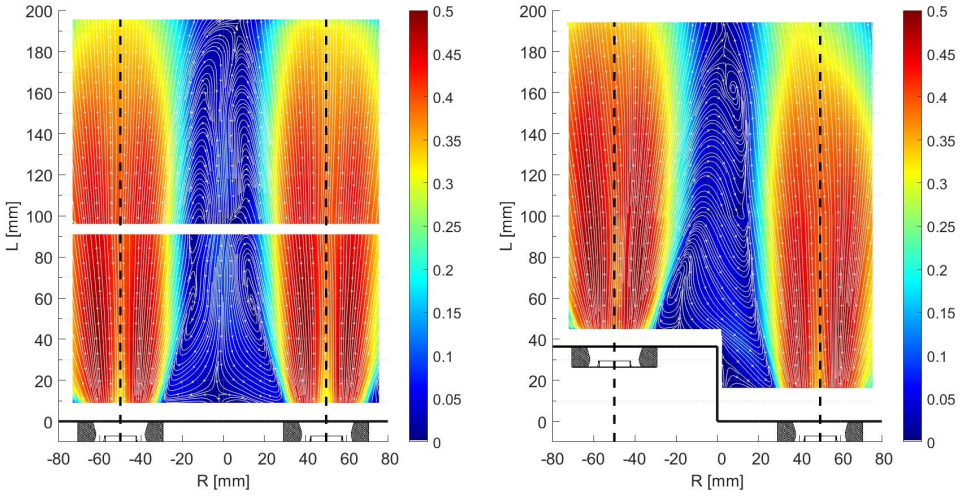

(a) Inline **(b)** Inclined (20°)

Figure 4.3: Contour of mean velocity magnitude overlaid with streamlines in the vertical axial mid-plane of the burners for different configurations.

reactive flow for the different alignments shown in Fig. 4.4 suggest an unexpected decrease in flow temperature of the inclined case near the wall which decreases the temperature at one side of ORZ due to the recirculated airflow from the upper burner to the lower one. The effect of the stepped wall in the inclined case on the recirculated flow between the adjacent burners is illustrated in more detail in Fig. 4.5.

According to these PIV measurements, there is a portion of the cold flow (shown by the green arrows in the schematic in Fig. 4.5b), moving from point 1 at the open side of the higher burner to point 2 near the wall of the lower

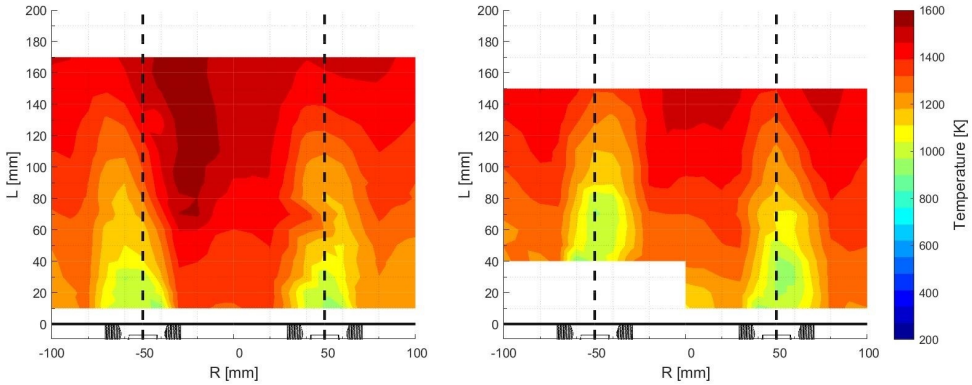

(a) Inline (0°) **(b)** Inclined (20°)

Figure 4.4: Contour plot of temperature distribution across the vertical nozzle mid plane for different configurations.

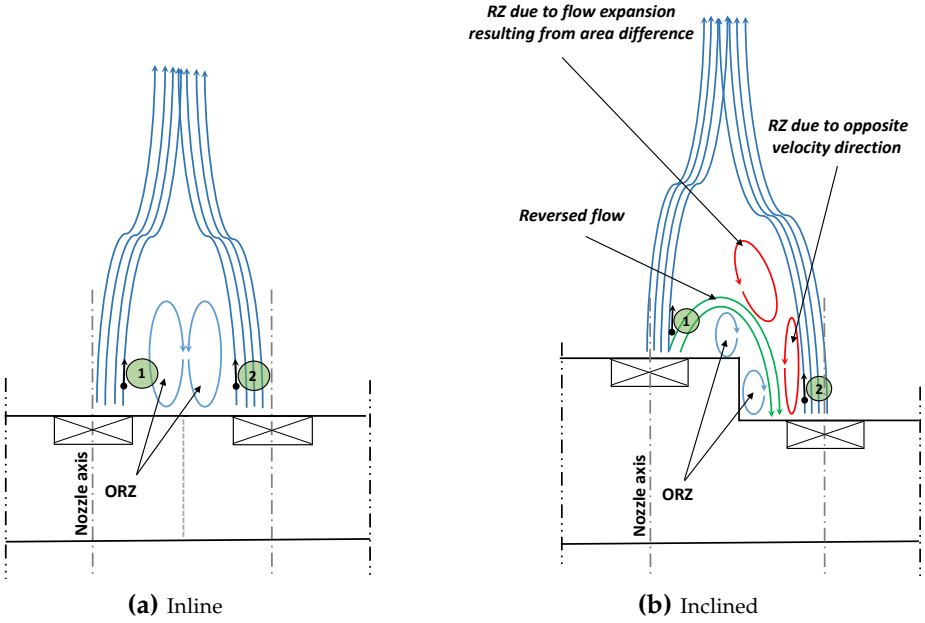

(a) Inline **(b)** Inclined

Figure 4.5: Qualitative schematic demonstrating the interaction between the outer recirculation zone (ORZ) and the flow in the adjacent sectors for different burner array arrangement.

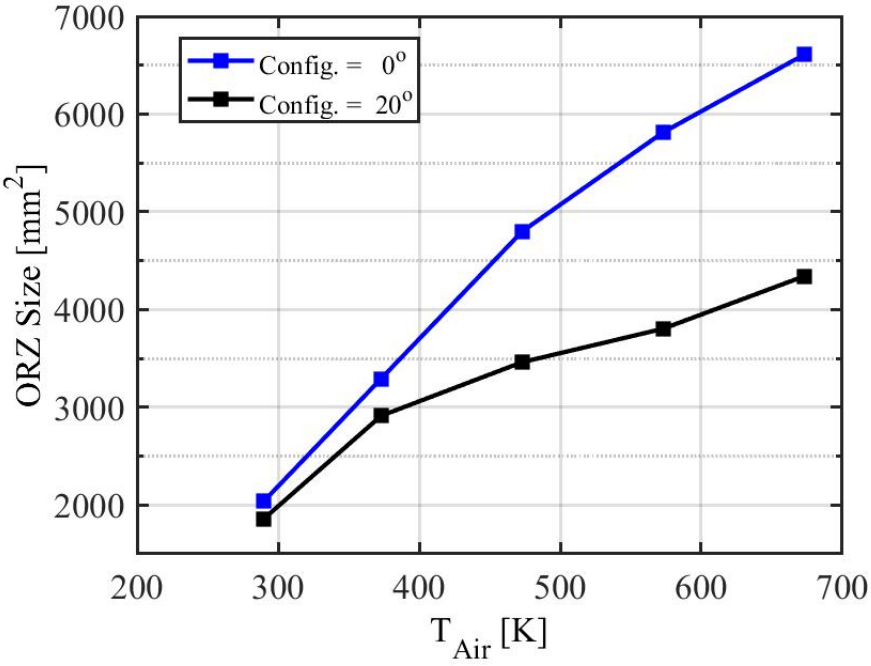

Figure 4.6: Effect of air inlet temperature (T_{Air}) on the size of the back-flow in the outer recirculation zone used as a characteristic indicator of the outer recirculation zone size for different burner array arrangements.

burner. This flow is driven by the pressure difference between free jet with low stream velocity and high pressure at the open side of the higher burner and confined jet with high stream velocity and low pressure) near the wall of the lower burner. This flow stream isolates the ORZ on the wall side and prevents it from contributing in the flame stabilization process. On the other side, there are another two small RZs (red arrows) that arise due to the flow expansion and differences in flow direction, which are induced by the ORZ near the wall and help the flame to stabilize.

4.1.3 Impact of the pressure drop across the nozzle

The impact of pressure drop across the nozzle on flame stability, at a constant air inlet temperature of 573 K, is depicted in Fig. 4.2 for various burner arrangements. In all the cases examined, an increase in pressure drop adversely affects flame stabilization, whether for the inline or inclined configurations. This relationship between air pressure drop and air inlet velocity can be expressed using the gas-dynamic equation, as follows ($\frac{\Delta P}{P_2} \propto {U_{gas}}^2$). As the pressure drop increases, so does the air velocity at crucial locations responsible for fuel atomization, such as the periphery of the pre-filmer rim. This increase in air velocity facilitates and enhances the process of fuel atomization. Consequently, it promotes rapid and thorough air/fuel mixing, particularly in the proximity of the burner dome. As a result, fast air/fuel mixing is achieved near the burner dome, and only a minor amount of non-evaporated droplets is present near to the nozzle axis and far away from the outer recirculation zone, which plays the dominant role in the flame stabilization of low swirl flames.

Understanding this complex interaction between pressure drop, air velocity, atomization, and flame stability is pivotal in optimizing this combustor concept.

4.2 Flame structure

Measurements of OH* chemiluminescence were performed at the axis of the central burner to qualitatively visualize the main reaction zone.

Fig. 4.7 presents an overview of the flame structure, illustrating the half-plane center burner flow field, the spatial distribution of the flame reaction zone (derived from Abel-transformed OH* chemiluminescence of 1000 averaged line-of-sight images), and the time-averaged fuel spray distribution for both inline and 20° inclined configurations. At low air inlet temperatures, OH* chemiluminescence images show outward distinct high-luminosity heat release regions on each side of the nozzle center, due to the outward moves of droplets near the shear layer attributed to the effect of lower T_{Air} that delays evaporation of the droplets. Fig. 4.7 depicts the time-averaged flame structures for each configuration under different T_{Air}, while Fig. 4.8 shows the instantaneous OH* distribution and fuel spray. By increasing T_{Air} the actual heat release region located more around the axis of the nozzle where fine fuel droplets with evaporated fuel accumulate and improved premixing with air takes place.

The flames are lifted for all investigated conditions as shown in . The flames are lifted for all investigated conditions, as shown in Fig. 4.7, which displays the right half of the flame, while the full flame is presented in the Appendix. The lift-off height (LOH) extends the time for evaporation and mixing. The lift-off height is defined as the distance from the jet outlet to the flame base. Lift-off height is of crucial importance, not only because of the direct impact on flame stabilization but also because can be used to explain the emission

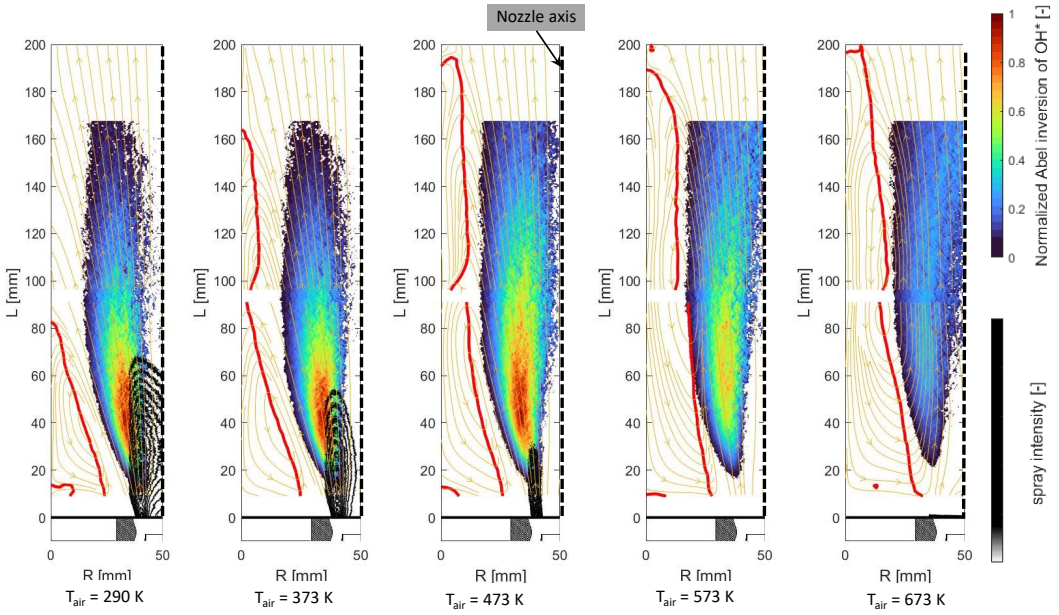

(a) Inline

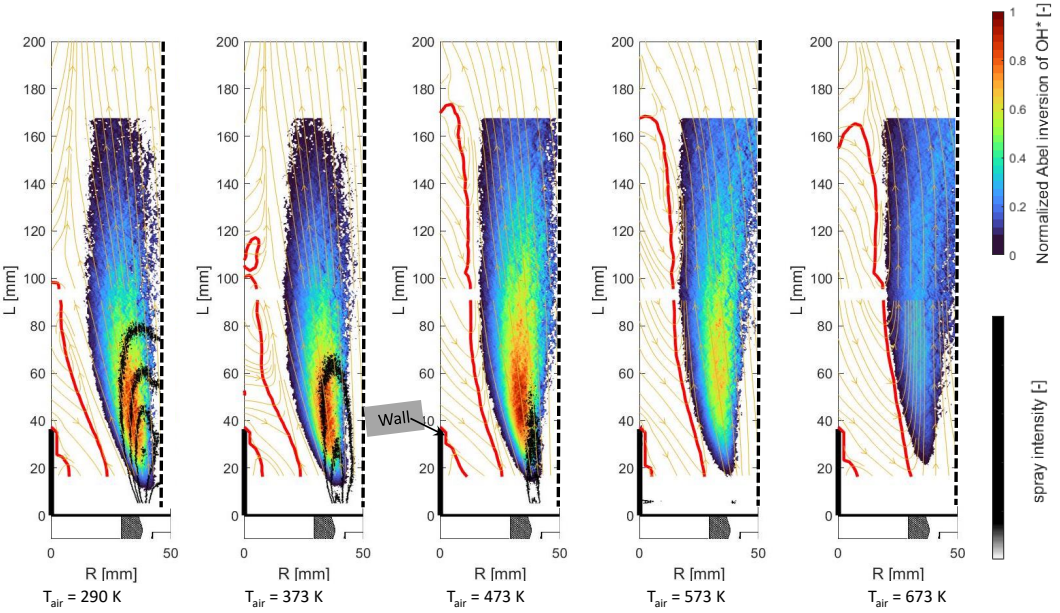

(b) Inclined (20°)

Figure 4.7: Contour plot of average OH* signal at constant ϕ=0.5 and $\frac{\Delta p}{P_2}$ = 3%, color contours show flame structure, black contours show fuel spray, red line shows the boundary of the back flow, yellow stream lines show axial velocity and black dash line shows nozzle center.

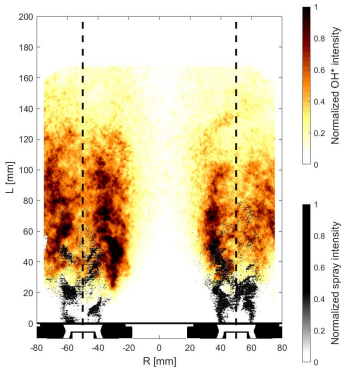

(a) Inline (θ = 0°), T_{Air} = 290K.

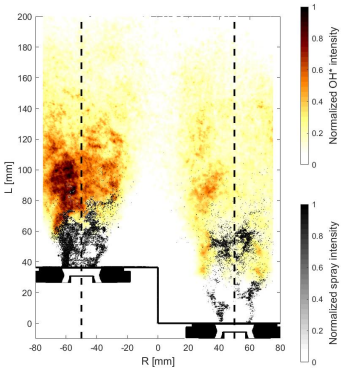

(b) Inclined (θ = 20°), T_{Air} = 290K.

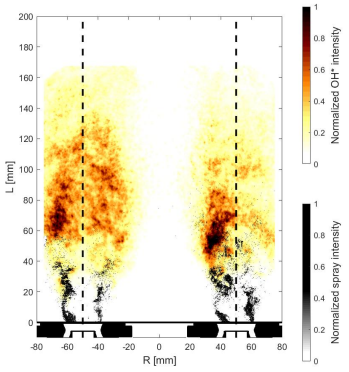

(c) Inline (θ = 0°), T_{Air} = 373K.

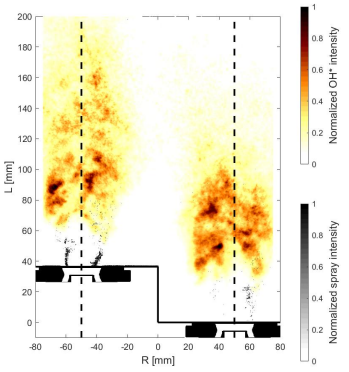

(d) Inclined (θ = 20°), T_{Air} = 373K.

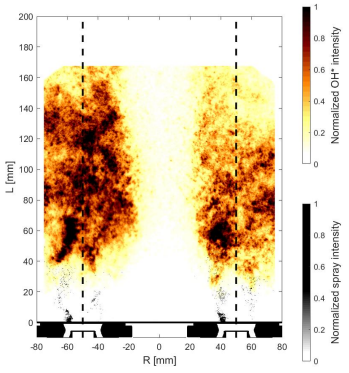

(e) Inline (θ = 0°), T_{Air} = 473K.

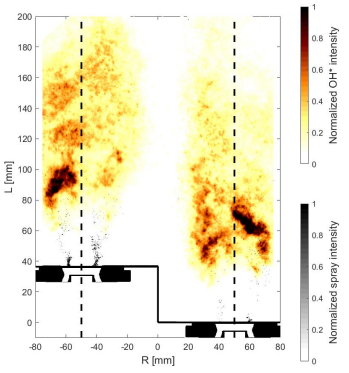

(f) Inclined (θ = 20°), T_{Air} = 473K.

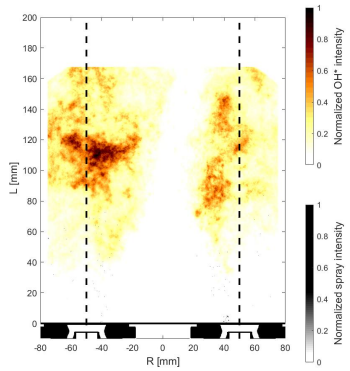

(g) Inline (θ = 0°), T_{Air} = 573K.

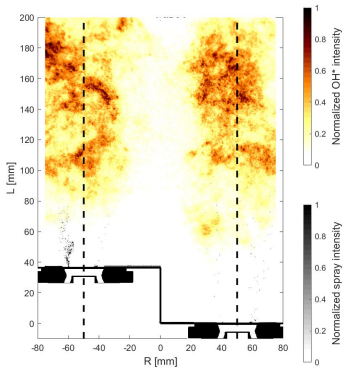

(h) Inclined (θ = 20°), T_{Air} = 573K.

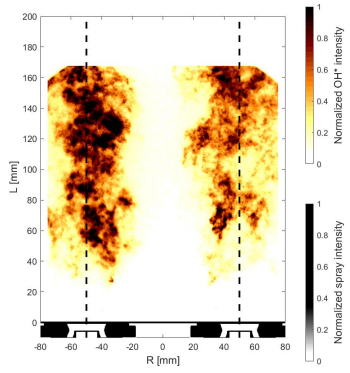

(i) Inline (θ = 0°), T_{Air} = 673K.

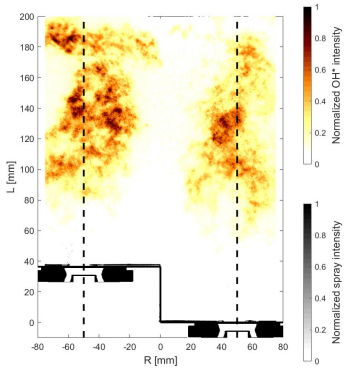

(j) Inclined (θ = 20°), T_{Air} = 673K.

Figure 4.8: Instantaneous contour plot of OH* signal and fuel spray contours (ϕ = 0.5, $\frac{\Delta p}{P_2}$ = 3%).

performance. In this study, the lift-off height was determined based on high speed OH* chemiluminescence measurements and defined as the distance between the nozzle exit and the horizontal line downstream of which 10% of the total chemiluminescence intensity is present as explained by [81, 82].

Fig. 4.9 shows the variations of lift-off height (LOH) with air inlet temperature studied for different configurations. It is evident that at lower temperatures and for all configurations, the flame stabilizes at a smaller distance above

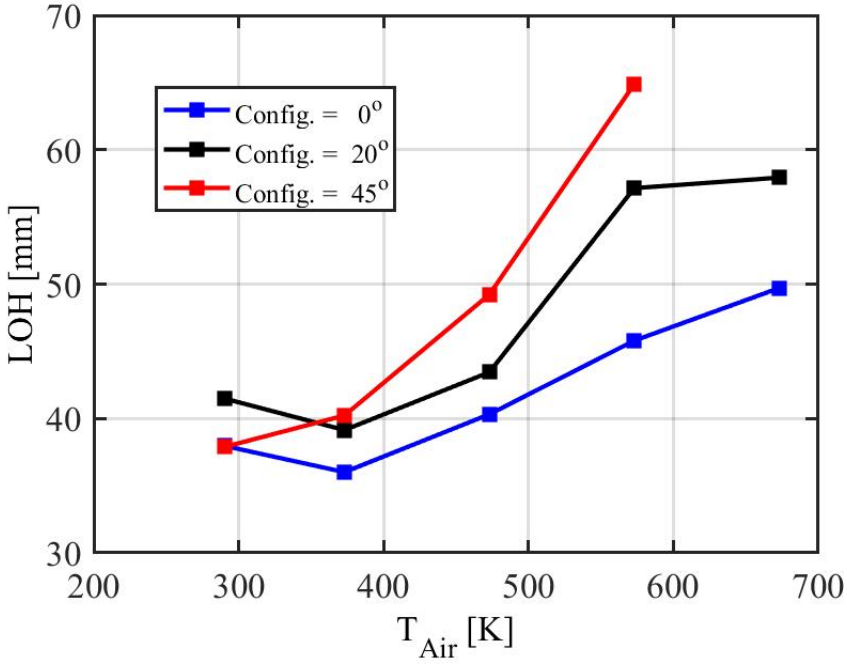

Figure 4.9: Effect of air inlet temperature T_{Air} on flame position/liftoff height for different burner array arrangement.

the nozzle exit resulting from the local rich pockets near the shear layer. For the same tilt angle, the flame lift-off height increases with increasing the air inlet temperature due to faster evaporation and the related higher degree of mixing. The higher degree of mixing is compatible with the mentioned stability mechanism in section 4.1. Increasing the air inlet temperature up to a certain point (based on each tilt angle) results in a decreased the ratio between the flow velocity and the burning velocity, causing the flame position to adapt and move upstream.

4.3 Emissions performance

In the previous section, the combustion characteristics, including the flame structure and stabilization mechanism, of helical and conventional annular modular combustor arrays were investigated at different operating conditions. To fully assess the innovative inclined combustor arrangement, the environmental impacts (i.e. Carbon monoxide (CO) and Nitrogen oxides (NO_x=NO+NO_2) emissions) for the steady state operating conditions were also recorded and analyzed under different operating conditions. The Emission Index (EI) as defined in SAE ARP 1533 guidelines [83] will be used to characterize the emission performance levels throughout this discussion. By directly comparing the global amount of each emissions species to that of the injected fuel, Figs. 4.10 and 4.11 depict the NO_x and CO emissions versus the equivalence ratio the adiabatic flame temperature for the inline (0° Config.) and the inclined (20° Config.) arrangements respectively. The adiabatic flame temperature was calculated using detailed chemistry for an equilibrium at defined pressure, air inlet temperature, fuel/air ratio and kerosene inlet temperature (constant at 293 K), taking into account the enthalpy of evaporation. Plotting EI versus T_{ad} allows better comparison of operating points with different air inlet temperature at similar combustion temperature assuming complete premixing. The differences in EI at the same T_{ad} can then be attributed to a different degree of premixing.

Fig. 4.10 shows the effects of air inlet temperature on the NO_x emissions of the inline and inclined configurations, where the same air inlet temperatures are shown in similar colors with solid and dashed lines for the inline and

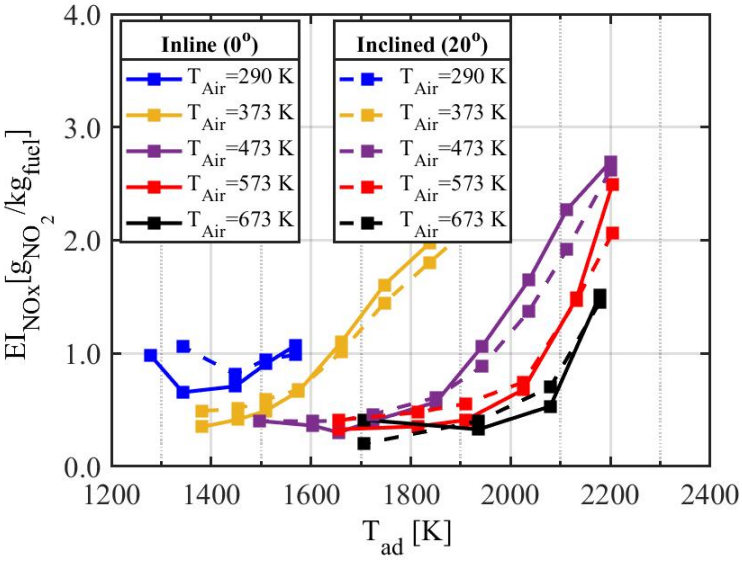

Figure 4.10: Impact of adiabatic flame temperature T_{ad} and the air preheating temperature T_{Air} on Emission Index of nitrogen oxides EI_{NO_x} on the at constant pressure drop across the nozzle of 3% for different burner array arrangement (Inline configuration shown in solid lines, Inclined configuration shown in dash lines).

inclined cases respectively. At low air inlet temperatures (290 K and 373 K) the fuel evaporation is rather slow with short LOH. Increasing the air inlet temperature (up to 473 K) rapidly lowers the overall NO_x emissions due to longer LOH, fast evaporation and related improvement of the homogeneity.

It is acknowledged that various mechanisms contribute to the formation of nitrogen oxides in gas turbines. The Zeldovich reactions are the primary source of NO_x production at high temperatures. This is supported by observations that a significant increase in adiabatic flame temperature leads to a corresponding increase in NO_x emissions for all examined configurations and conditions. It can be also seen that the inclined configuration has slightly better NO_x emission performance near to the high temperature conditions as

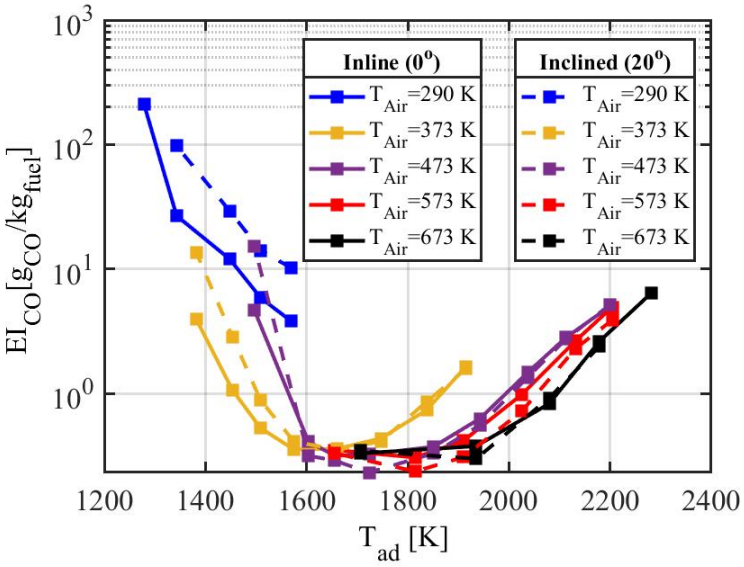

Figure 4.11: Impact of adiabatic flame temperature T_{ad} and the air preheating temperature T_{Air} on Emission Index of carbon monoxide EI_{CO} on the at constant pressure drop across the nozzle of 3% for different burner array arrangement (Inline configuration shown in solid lines, Inclined configuration shown in dash lines).

shown in Fig. 4.10 due to the long LOH. A potential reason for the limited improvement is that the smaller outer recirculation in the inclined case may constrain the emission reduction.The CO emissions are shown in Fig. 4.11 for the same operating points as the NO_x emissions. If the adiabatic combustion temperature is reduced further after the steep increase of CO, the flame blows off. At low inlet temperatures, The flame is partly quenched and the CO emissions are just rising steadily before flame extinction. At higher combustion temperatures the EI_{CO} emissions rise again due to equilibrium concentration for CO and CO_2.

4.4 Ion probe diagnostics

Ion current measurements have been used in several studies as flame indicator to detect the reaction rate. The ion probe measurement system was installed at the multi-burner configuration (20 ° configuration) as shown in Fig. 3.12. The ion current measurement system consists of the water cooled probe, a DC power supply, an isolating amplifier and a signal analyzer. At the platinum sphere the DC power supply applies a voltage of 150 V. The water cooled ion current probe was inserted from top.

In this experimental investigation field measurements of the ion concentration with a sampling rate of 30 kHz was used. As presented Wollgarten et al. by [84], the signal obtained from an ion current detector inside a combustor depends strongly on the measurement position. Therefore, results from two positions are presented in this investigations as shown in Fig. 4.12. One position is near to the wall, which could be a position of an igniter serving as ion probe, and the other position is located between 2 burners to study the effect of flame interaction signal related to ion concentration.

Variations in the air-to-fuel ratio (AFR) and air preheating temperature (T_{Air}) were investigated to assess their impact on the ion current signal. As we can see from Fig. 4.13 by decreasing the equivalence ratio the RMS value of the ion current signal decreases significantly for all investigated conditions/locations. The position of the probe significantly impacts the RMS value of the ion current signal, with higher values observed in the flame interaction region compared to point 2 near the wall, due to the mixing of flows between the two neighboring flames.

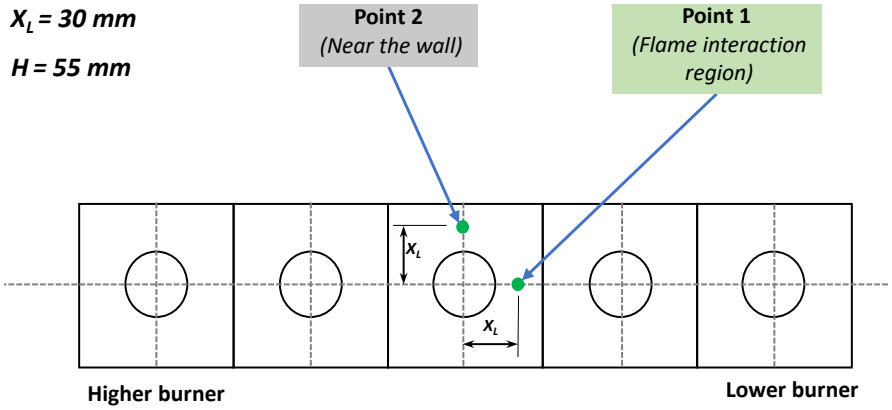

Figure 4.12: Positions of ion probe measurements investigations.

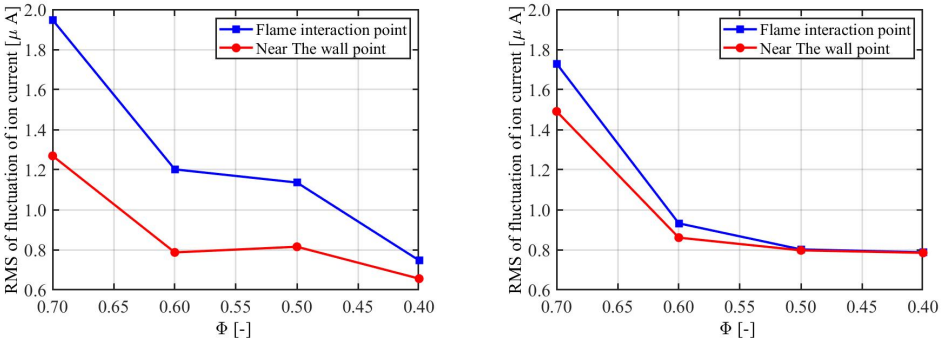

(a) T_{Air} = 290K. **(b)** T_{Air} = 673K.

Figure 4.13: RMS ion current correlates with the equivalence ratio, measurement frequency (30 kHz), threshold= 0.7 μA for inclined configuration (θ = 20°) at different air inlet temperature.

The experiment was run for 5 minutes, during which data was collected. The time between ion current peaks correlates with the equivalence ratio, with a measurement frequency of 30 kHz. A threshold of 0.7 µA was used to filter out peaks lower than this value. The data shows that, at the start of the experiment, when the equivalence ratio is higher and the flame is stable, the time between peaks is shorter. However, as the equivalence ratio decreases toward lean blowout (LBO), the flame becomes unstable and starts pulsating. This results in an increasing time between peaks in the probe's region until flame blowout occurs as shown in Fig. 4.14. The sudden increase of the timescale between the ion current fluctuations peaks just before the LBO of the flame which could be used as a control to detect the conditions near to the LBO conditions in an engine and to ensure flame stability.

In order to gain a deeper understanding of the behavior of the ion current signal, the ion current was mapped in both the normal (x) and parallel (y) directions using the same ion probe tool. This mapping was specifically

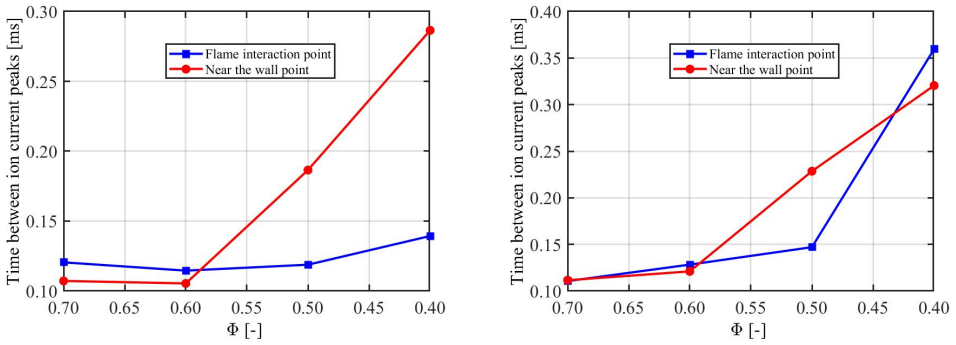

(a) T_{Air} = 290K. **(b)** T_{Air} = 673K.

Figure 4.14: Time between ion current peaks correlates with the equivalence ratio, measurement frequency (30 kHz), threshold= 0.7 μA for inclined configuration (θ = 20°) at different air inlet temperature.

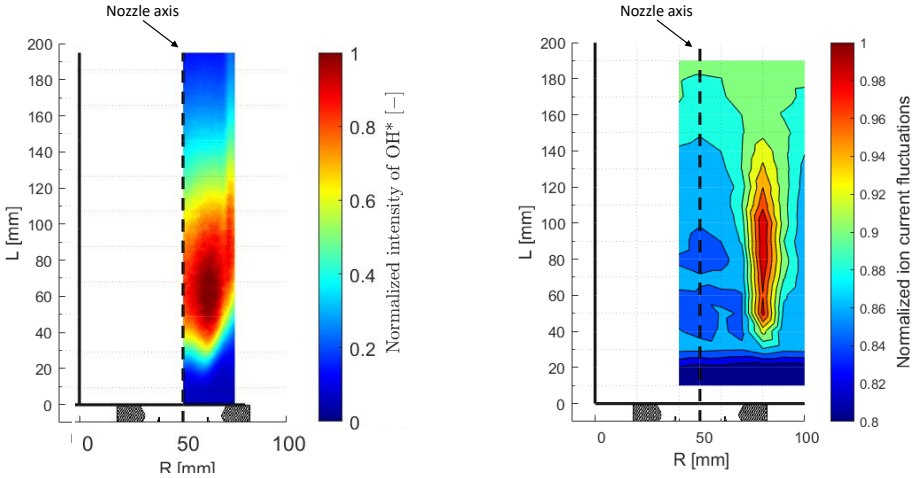

(a) Abel-transformed OH* chemiluminescence. **(b)** RMS ion current.

Figure 4.15: Comparison of normalized ion current fluctuation and OH* measurements in the left half of the middle flame for the inclined configuration, (θ = 20°), T_{Air} = 290K and dp/p of 3%.

conducted within the left half of the middle flame for the inclined configuration, resulting in ion current signal contour maps with a cell length of 1 cm. The root mean square of the ion current fluctuations was then compared to OH* chemiluminescence measurements under identical operating conditions, specifically a T_{Air} of 290K and dp/p of 3%. Fig. 4.15 shows the comparison of the normalized ion current fluctuation and OH* measurements revealed a high degree of correlation, indicating that the ion current can serve as a reliable diagnostic tool for the study of reaction zones. This finding is supported by the fact that the contour maps of the ion current fluctuation (I_{rms}) closely match those of the OH* measurements, providing evidence for the applicability of ion current measurements in this context.

4.5 Discussion of the main findings

This study explored the effects of burner inclination angles on the stabilization mechanisms, flame structure, and emission characteristics of kerosene/air flames in a multi-burner setup under lean conditions. The investigated multi burner arrays with lean lifted spray flames with low swirl has shown a remarkable stability limit compared to other lean injection system with higher swirl as well as very low NO_x emissions. This finding is valid for all investigated inclination angles.

At low air inlet temperatures, both the inline and inclined configurations exhibited good flame stability due to the slow evaporation of fuel droplets, which led to the formation of locally rich pockets near the flame root. This was also linked to a lower lift-off height, resulting in the flame stabilizing upstream close to the burner dome with short lift-off height.

At elevated air inlet temperatures, analyses unexpectedly revealed that the inline burner configuration demonstrated slightly higher stability compared to the inclined configuration, relying on different flame stabilization mechanisms. In the inline arrangement, the flame stabilization was primarily influenced by Outer Recirculation Zones (ORZs) located at the sides of each burner. The size and position of these ORZs depended on the ratio of air inlet temperature to adiabatic flame temperature, which significantly affected the flow expansion within the combustor. These recirculation zones not only anchored the flame but also enhanced the mixing of fresh gases with burnt gases, thereby increasing turbulence—key factors for flame stabilization.

Conversely, in the inclined configuration, temperature profiles unexpectedly showed a decrease in flow temperature near the wall. This decrease occurred due to recirculated airflow from the upper burner to the lower one, driven by the pressure difference between the free jet with low stream velocity and high pressure at the open side of the higher burner, and the confined jet with high stream velocity and low pressure near the wall of the lower burner. This airflow isolates the ORZ on the wall side, preventing it from contributing to the flame stabilization process, thereby reducing flame stability. However, two smaller recirculation zones (RZs) emerge due to flow expansion and differences in flow direction induced by the ORZ near the wall. These smaller RZs aid in stabilizing the flame, suggesting potential for future research to improve flame stability in the inclined configuration by modifying the shape of the side wall to leverage the benefits of these smaller RZs while mitigating the disadvantages of the cold airflow moving from the upper to the lower burner. Similar observations were made regarding flame location and lift-off height, where the lift-off height increased with increasing inclination angle, improving premixing but consequently reducing flame stability. As the air inlet temperature further increased, the ratio between flow velocity and burning velocity decreased, causing the flame position to move upstream, thereby enhancing flame stability once again. Consequently, the inclined burner configuration demonstrated potential for lower NO_x emissions under high-temperature operating conditions.

Chapter 5

Summary and outlook

The primary objective of this investigation is to assess the operational performance of a gas turbine model combustor equipped with a lean fuel combustion system operating with liquid fuel. The core goal is to gain an in-depth understanding of flame behavior, stability factors, and emission performance across various operating scenarios. In this concept, lean lifted flames are combined with Short Helical Combustors (SHC) by tilting the axis of the flames relative to the turbine axis to enhance the interaction of adjacent flames in a circumferential direction. An extensive series of experimental tests were conducted at a multi-burner array test rig. These tests involved varying several key parameters, including the tilt angles of burners (θ), equivalence ratios (ϕ), relative air pressure drops across the nozzle ($\frac{\Delta p}{p1}$), which is representative of the air mass flow rate, and air inlet temperatures (T_{Air}) under ambient pressure conditions.

The experimental campaign employed advanced optical diagnostic techniques, including Particle Image Velocimetry (PIV) for spatially resolved flow field measurements, Mie scattering for qualitative analyses of the fuel spray penetration, and OH* chemiluminescence for capturing flame structure. Additionally, probe measurements provided critical data on temperature profiles and emission concentrations. The experimental operating conditions were selected to closely mimic those found in real-world aeronautic propulsion systems, specifically regarding the combustor/nozzle relative sizes and the elevated air inlet temperature, which reaches up to 673 K. However, the interesting aspect of this work lies in utilizing low swirl combustion with lifted flames.

The results show that the low swirl flames (SN=0.47) under investigation exhibit remarkable stability compared to higher swirl flames (SN=0.76), which are characterized by larger inner recirculation zones. These low swirl flames create outer recirculation zones (ORZs) due to the entrainment of surrounding fluid by the low-swirl, high-velocity flow. The ORZs significantly enhance flame stability by transporting reactive species back to the nozzle in an upstream direction, making outer recirculation the dominant stabilization mechanism. The investigated low swirl lean lifted flames demonstrate significant potential for reducing NO_x emissions. Additionally, the results suggest that the same combustion concept could be applied to an inclined configuration, as the low swirl can reduce unwanted flow deflection and offers beneficial flow characteristics.

Slight differences in flame stability and emission performance were observed between the inline and inclined configurations, each utilizing different stabilization mechanisms. At high air inlet temperatures, surprisingly, analyses

indicated that the inline arrangement of burners demonstrated slightly higher stability when compared to the inclined configuration. These two configurations relied on different flame stabilization mechanisms. In the case of the inline arrangement, the flow field structure was found to be dominated by ORZs located at the sides of each individual burner. The size and location of these ORZs were found to be dependent on the ratio of air inlet temperature to adiabatic flame temperature, which played a decisive role in determining the flow expansion inside the combustor. These recirculation zones, besides serving as sites for flame anchoring, facilitating enhanced mixing of fresh gases with the already burnt gases, and heightened turbulence levels—factors crucial for flame stabilization. Conversely, in the inclined configuration, temperature profiles revealed an unexpected decrease in flow temperature near the wall. This phenomenon occurred due to the recirculated airflow from the upper burner to the lower one, affecting the temperature on one side of the ORZ.

Notably, at low air inlet temperatures a distinct flame stabilization mechanism became apparent. This mechanism was driven by the slow evaporation of fuel droplets, which resulted in the formation of local rich pockets near the flame root. Remarkably, this phenomenon was observed for both inline and inclined configurations.

The utilization of OH* chemiluminescence and Mie scattering techniques provides insights into the size and location of heat release rate variations under different operating conditions. At lower air inlet temperatures, OH* chemiluminescence images reveal outwards distinct high-luminosity heat release regions on each side of the nozzle. This phenomenon results from the outward movement of droplets near the shear layer between the IRZ and ORZ,

influenced by lower air inlet temperatures that delay droplet evaporation. Additionally, the results demonstrate that at lower temperatures, regardless of configuration, the flame stabilizes at a shorter distance above the nozzle exit due to the presence of local rich pockets near the shear layer. For the same tilt angle, the flame lift-off height increases with rising air inlet temperatures, driven by faster evaporation and higher degrees of lean premixing, and high inlet velocity.

Exhaust gas analyses were conducted to evaluate the emission performance of the multi-burner arrangement. The findings indicate that lifted flames yield very low NO_x emissions across a wide range of operating conditions for all configurations investigated, compared to the moderate swirl typically used in aero-engines. The inclined configuration exhibited lower emissions at higher air inlet temperatures compared to the inline configurations.

Ion probe techniques have been employed in inclined configurations at various locations to predict conditions approaching Lean Blowout (LBO) by analyzing the root mean square (RMS) of the ion current generated within the flame. Measurements were taken at two critical points: between the burners and near the wall. The RMS values of the ion current signal were higher in the flame interaction region compared to those near the wall. Additionally, results demonstrated a significant increase in the time between ion current fluctuations just before LBO, underscoring its potential as a control parameter for maintaining engine flame stability. The strong correlations between ion current measurements and traditional OH* measurements further confirm the reliability and effectiveness of ion current as a simple diagnostic tool, especially under low air inlet temperature conditions.

In summary, these findings advance the development and optimization of lean combustion technology for aircraft engines. The research demonstrates that lifted low-swirl flames consistently exhibit low NO_x emissions across a broad range of operational conditions for all configurations analyzed. It suggests that the same combustion concept could be effectively applied to inclined configurations, as low swirl mitigates unwanted flow deflection and provides a slight deflection in the beneficial direction for the turbine inlet conditions. The study also shows to the potential for further improvement by adjusting the shape and size of the sidewall in the helical arrangement to optimize recirculation zones. Future research could explore this concept under higher pressure conditions, similar to realistic engine settings, and investigate the impact of auto-ignition on stabilization in inclined cases. Additionally, refining the swirl number and examining the relative swirl direction of adjacent burners may yield further advancements.

Appendix

This appendix provides detailed figures and contour plots of velocity and flame interactions from the experimental investigation conducted at different air inlet temperatures and burner arrangements. The figures provide a comprehensive view of the velocity fields for both reactive and non-reactive flows under various configurations. The data presented here supports the findings discussed in the main body of the thesis.

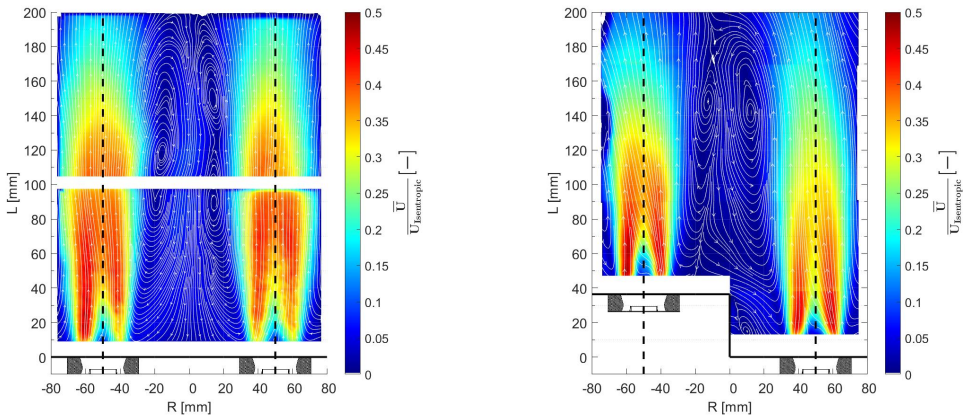

(a) Inline (θ =0°). **(b)** Inclined (θ =20°).

Figure A1.2: Normalized average velocity ($\overline{U} = \sqrt{u_x^2 + u_y^2}$) field of the non-reactive swirling flow in the central cross section of the model burner array.

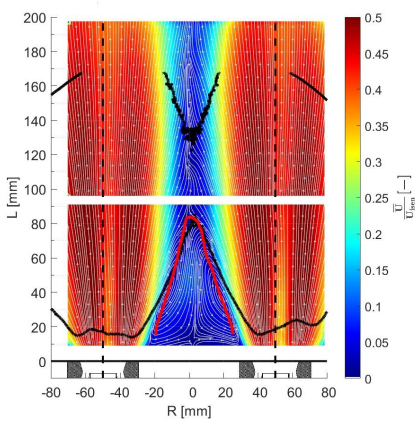

(a) Inline (θ = 0°), T_{Air} = 290K.

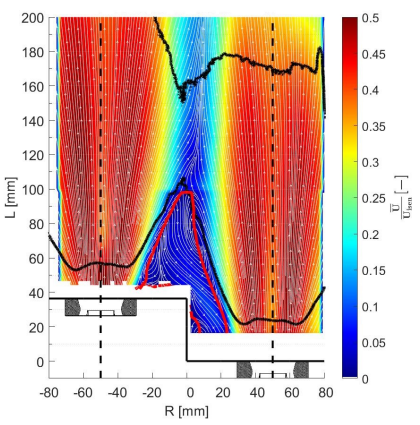

(b) Inclined (θ = 20°), T_{Air} = 290K.

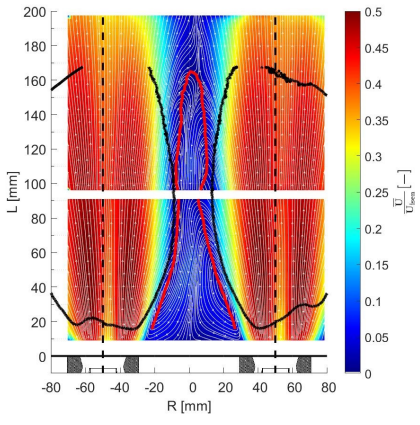

(c) Inline (θ = 0°), T_{Air} = 373K.

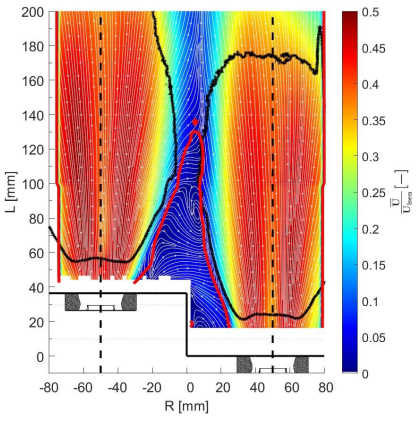

(d) Inclined (θ = 20°), T_{Air} = 373K.

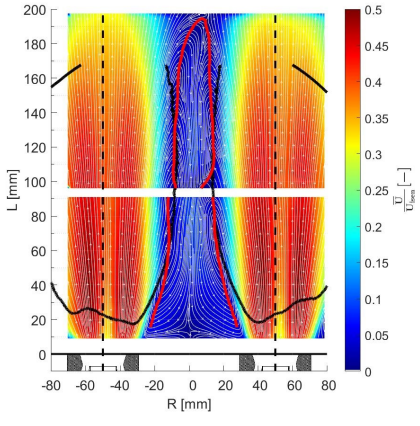

(e) Inline (θ = 0°), T_{Air} = 473K.

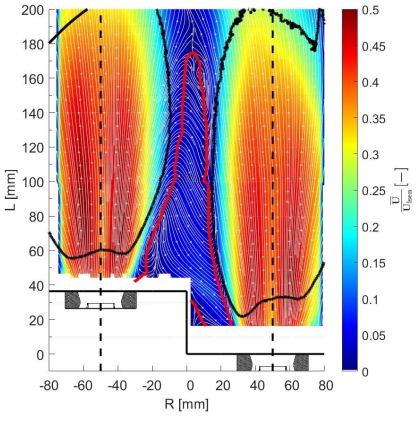

(f) Inclined (θ = 20°), T_{Air} = 473K.

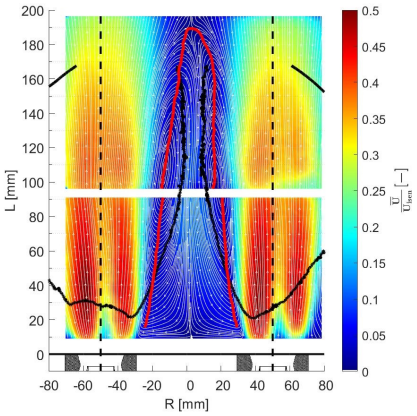

(g) Inline (θ = 0°), T_{Air} = 573K.

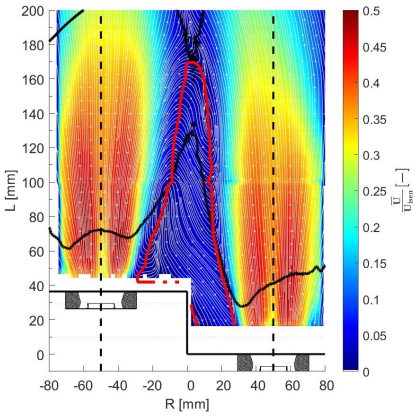

(h) Inclined (θ = 20°), T_{Air} = 573K.

Figure A1.3: Contour plot of time average velocity (1000 single-shot recorded at 5 kHz) at constant equivalence ratio and pressure drop across the nozzle respectively ϕ=0.5, $\frac{\Delta p}{P_2}$ = 3% to study the impact of air inlet temperature T_{Air} for different arrangement, where black solid line shows the flame root, solid red line represents the outer recirculation zone, and the black dash line shows the center of each nozzle.

Chapter 6

Bibliography

[1] A. Kalantari and V. McDonell: *Boundary layer flashback of non-swirling premixed flames: Mechanisms, fundamental research, and recent advances*. Progress in Energy and Combustion Science 61 (2017).

[2] F. Joos: *Technische Verbrennung*. Vol. 76. Springer, 2006.

[3] *International Energy Outlook 2013*. Tech. rep. U.S. Energy Information Administration, 2013.

[4] Y. Liu, X. Sun, V. Sethi, D. Nalianda, Y.-G. Li, and L. Wang: *Review of modern low emissions combustion technologies for aero gas turbine engines*. Progress in Aerospace Sciences 94 (2017).

[5] T. Boningari and P. G. Smirniotis: *Impact of nitrogen oxides on the environment and human health: Mn-based materials for the NOx abatement*. Current Opinion in Chemical Engineering 13 (2016).

[6] I. Secretariat: *Annex 16—environmental protection volume II—aircraft engine emissions*. Tech. rep. ISBN 978-92-9231-123-02008, 2008.

[7] E. Commission, D.-G. for Mobility, Transport, D.-G. for Research, and Innovation: *Flightpath 2050 : Europe's vision for aviation : maintaining global leadership and serving society's needs*. Publications Office, 2011.

[8] J. Warnatz, U. Maas, R. W. Dibble, and J. Warnatz: *Combustion*. Springer, 2006.

[9] Y. B. Zeldvich: *The oxidation of nitrogen in combustion and explosions*. J. Acta Physicochimica 21 (1946).

[10] C. K. Law: *Combustion physics*. Cambridge university press, 2010.

[11] A. H. Lefebvre and D. R. Ballal: *Gas turbine combustion: alternative fuels and emissions*. CRC press, 2010.

[12] J. Bullermann, N.-C. Meyer, A. Krafft, and F. Wirz: *Comparison of fuel properties of alternative drop-in fuels with standard marine diesel and the effects of their blends*. Fuel 357 (2024).

[13] T. Poinsot and D. Veynante: *Theoretical and numerical combustion, RT Edwards Inc*. Philadelphia, PA (2001).

[14] S. No, J. Gu, H. Moon, C. Lee, and Y. Jo: *An introduction to combustion concepts and applications*. (2011).

[15] T. Echekki and E. Mastorakos: *Turbulent combustion modeling: Advances, new trends and perspectives* (2010).

[16] A. H. Lefebvre and V. G. McDonell: *Atomization and sprays*. CRC press, 2017.

[17] D. Veynante and L. Vervisch: *Turbulent combustion modeling*. Progress in energy and combustion science 28.3 (2002).

[18] A. K. Gupta, D. G. Lilley, and N. Syred: *Swirl flows*. Tunbridge Wells (1984).

[19] F. El-Mahallawy and S.-D. Habik: *Fundamentals and technology of combustion*. Elsevier, 2002.

[20] D. Dunn-Rankin: *Lean combustion: technology and control*. Academic Press, 2011.

[21] F. A. Williams: *Combustion theory*. CRC Press, 2018.

[22] M. Lackner, F. Winter, and A. K. Agarwal: *Handbook of combustion*. Methods 1.4 (2013).

[23] N. Peters: *Combustion theory*. RWTH Aachen University (CEFRC Summer School) (2010).

[24] E. Mallard: *Recherches experimentales et theoriques sur la combustion des melanges gaseux explosifs*. Ann. mines 8.4 (1883).

[25] G. Damköhler: *Der einfluss der turbulenz auf die flammengeschwindigkeit in gasgemischen*. Zeitschrift für Elektrochemie und angewandte physikalische Chemie 46.11 (1940).

[26] C. Tanford and R. N. Pease: *Theory of burning velocity. II. The square root law for burning velocity*. The Journal of Chemical Physics 15.12 (1947).

[27] Y. B. Zeldovich, G. Barenblatt, V. Librovich, and G. Makhviladze: *The Mathematical Theory of Combustion and Explosions, Consultants Bureau, New York, 1985*. C101, C102, C103, C106 References C115 Author addresses 1 (1960).

[28] *CHEMKIN Tutorials Manual*. CHEMKIN Software, CK-TUT-10112-1112-UG-1. Reaction Design. San Diego, 2011.

[29] H. Pitsch: *Combustion theory and applications in CFD*. Lecture note, Tsinghua-Princeton Summer School on Combustion. Tsinghua University, Beijing, China (2015).

[30] R. Mahmoud: *Development and Application of an Eulerian Density Function Methodology coupled to Flamelet Progress Variable Approach for the Simulation of Oxyfuel Combustion*. PhD thesis. université Paris-Saclay, 2020.

[31] R. Borghi, C. Bruno, and C. Casci: *Recent advances in aeronautical science*. Pergamont, London, UK (1984).

[32] N. Peters: *The turbulent burning velocity for large-scale and small-scale turbulence*. Journal of Fluid mechanics 384 (1999).

[33] B. Ariatabar, R. Koch, H.-J. Bauer, and D.-A. Negulescu: *Short helical combustor: Concept study of an innovative gas turbine combustor with angular air supply*. Journal of Engineering for Gas Turbines and Power 138.3 (2016).

[34] S. Chung and B. Lee: *On the characteristics of laminar lifted flames in a nonpremixed jet*. Combustion and Flame 86.1-2 (1991).

[35] S. Chung: *Stabilization, propagation and instability of tribrachial triple flames*. Proceedings of the Combustion Institute 31.1 (2007).

[36] B. Lee and S. Chung: *Stabilization of lifted tribrachial flames in a laminar nonpremixed jet*. Combustion and Flame 109.1-2 (1997).

[37] C. S. Yoo, R. Sankaran, and J. Chen: *Three-dimensional direct numerical simulation of a turbulent lifted hydrogen jet flame in heated coflow: flame stabilization and structure*. Journal of Fluid Mechanics 640 (2009).

[38] N. Syred and J. Beer: *Combustion in swirling flows: a review*. Combustion and flame 23.2 (1974).

[39] D. Spalding: *Combustion Aerodynamics. By JM BEéER and NA CHIGIER. Applied Science Publishers Ltd, 1972. 264 pp.£ 7.00.* Journal of Fluid Mechanics 54.4 (1972).

[40] P. Maier: *Untersuchung turbulenter isothermer Drallstrahlen und turbulenter Drallflammen*. German. PhD thesis. 1967.

[41] N. Zarzalis, P. Fokaides, and K. Merkle: *Fuel injection apparatus*. Patent No. DE 10 (2005).

[42] P. Kasabov, N. Zarzalis, and P. Habisreuther: *Experimental study on lifted flames operated with liquid kerosene at elevated pressure and stabilized by outer recirculation*. Flow, turbulence and combustion 90.3 (2013).

[43] R. S. Hall: *Spiral annular combustion chamber*. US Patent 3,000,183. (1961).

[44] S. Burd and A. Cheung: *Angled flow annular combustor for turbine engine*. WO Patent Application PCT/US2006/007,898 (2007).

[45] A. A. Mancini, D. L. Burrus, and S. J. Lohmueller: *Method and apparatus for assembling gas turbine engine*. US Patent 7,716,931. (2010).

[46] S. Sohrab, Z. Ye, and C. Law: *An experimental investigation on flame interaction and the existence of negative flame speeds*. *Symposium (International) on Combustion*. Vol. 20. 1. Elsevier. 1985.

[47] B. Dolan, R. V. Gomez, and E. Gutmark: *Optical measurements of interacting lean direct injection fuel nozzles with varying spacing*. *Turbo Expo: Power for Land, Sea, and Air*. Vol. 56697. American Society of Mechanical Engineers. 2015.

[48] B. Dolan, R. Villalva Gomez, H. Nawroth, S. Pack, and E. Gutmark: *Study on the isothermal flowfields of interacting swirl-stabilized nozzles*. *Proceedings of the 53rd AIAA Aerospace Sciences Meeting, Kissimmee, FL, USA*. 2015.

[49] J. Kariuki, N. Worth, J. Dawson, and E. Mastorakos: *Visualisation of blow-off events of two interacting turbulent premixed flames*. *51st AIAA Aerospace Sciences Meeting including the New Horizons Forum and Aerospace Exposition*. 2013.

[50] W. Y. Kwong and A. M. Steinberg: *Blowoff and reattachment dynamics of a linear multinozzle combustor*. Journal of Engineering for Gas Turbines and Power 141.1 (2019).

[51] C. Kraus, S. Harth, and H. Bockhorn: *Experimental investigation of combustion instabilities in lean swirl-stabilized partially-premixed flames in single-and multiple-burner setup*. International Journal of Spray and Combustion Dynamics 8.1 (2016).

[52] M. Rachner: *Die stoffeigenschaften von kerosin jet a-1*. DLR-Mitteilungen 98-01 1 (1998).

[53] P. Kasabov and N. Zarzalis: *Pressure dependence of the stability limits and the NOx exhaust gas concentrations in case of swirl-stabilized, diffusion flames burning in a lift-off regime*. *Turbo Expo: Power for Land, Sea, and Air*. Vol. 48838. 2009.

[54] J. C. Wollgarten, N. Zarzalis, F. Turrini, and A. Peschiulli: *Experimental investigations of ion current in liquid-fuelled gas turbine combustors*. International Journal of Spray and Combustion Dynamics 9.3 (2017).

[55] K. R. Adhikari: *Thermocouple: facts and theories*. Himalayan Physics (2017).

[56] J. Lawton: *Electrical aspects of combustion*. Clarenton (1969).

[57] I. Langmuir and H. Mott-Smith: *Studies of electric discharges in gases at low pressures*. General Electric Review 27.12 (1924).

[58] A. B. Fialkov: *Investigations on ions in flames*. Progress in energy and combustion science 23.5-6 (1997).

[59] G. Wortberg: *Ion-concentration measurements in a flat flame at atmospheric pressure*. *Symposium (International) on Combustion*. Vol. 10. 1. Elsevier. 1965.

[60] H. Calcote, S. Kurzius, and W. Miller: *Negative and secondary ion formation in low-pressure flames*. *Symposium (International) on Combustion*. Vol. 10. 1. Elsevier. 1965.

[61] M. Ahlheim: *Reaktionsstruktur einer turbulenten Diffusionsflamme hergeleitet aus Ionisationsmessungen*. na, 1980.

[62] H. Hoffmann: *Turbulente Bunsenflammen: Struktur u. Flammengeschwindigkeit*. na, 1986.

[63] W. Kohler: *Turbulenz und Turbulenzstruktur in freien und eingeschlossenen Flammen*. na, 1988.

[64] R. Balachandran, B. Ayoola, C. Kaminski, A. Dowling, and E. Mastorakos: *Experimental investigation of the nonlinear response of turbulent premixed flames to imposed inlet velocity oscillations*. Combustion and Flame 143.1-2 (2005).

[65] T. Kathrotia, U. Riedel, and J. Warnatz: *A numerical study on the relation of OH*, CH*, and C2* chemiluminescence and heat release in premixed methane flames*. *Proceedings of the European combustion Meeting*. Vol. 2009. 2009.

[66] Y. Liu, J. Tan, M. Wan, L. Zhang, and X. Yao: *Quantitative measurement of OH* and CH* chemiluminescence in jet diffusion flames*. ACS omega 5.26 (2020).

[67] A. G. Gaydon: *The spectroscopy of flames*. Wiley: New York, 1974.

[68] M. R. W. Lauer: *Determination of the heat release distribution in turbulent flames by chemiluminescence imaging*. PhD thesis. Technische Universität München, 2011.

[69] V. Nori and J. Seitzman: *Chemiluminescence measurements and modeling in syngas, methane and jet-A fueled combustors*. *45th AIAA Aerospace Sciences Meeting and Exhibit*. 2007.

[70] H. N. Najm, P. H. Paul, C. J. Mueller, and P. S. Wyckoff: *On the adequacy of certain experimental observables as measurements of flame burning rate*. Combustion and flame 113.3 (1998).

[71] J. Lee and D. Santavicca: *Experimental diagnostics for the study of combustion instabilities in lean premixed combustors*. Journal of propulsion and power 19.5 (2003).

[72] Y. Hardalupas and M. Orain: *Local measurements of the time-dependent heat release rate and equivalence ratio using chemiluminescent emission from a flame*. Combustion and Flame 139.3 (2004).

[73] B. Ayoola, R. Balachandran, J. Frank, E. Mastorakos, and C. Kaminski: *Spatially resolved heat release rate measurements in turbulent premixed flames*. Combustion and flame 144.1-2 (2006).

[74] S. Jaffe, J. Larjo, and R. Henberg: *Abel inversion using the fast Fourier transform. 10th International Symposium on Plasma Chemistry*. 1991.

[75] M. Atkins: "Velocity field measurement using particle image velocimetry (PIV)". *Application of Thermo-Fluidic Measurement Techniques*. Elsevier, 2016.

[76] C. E. Willert and M. Gharib: *Digital particle image velocimetry*. Experiments in fluids 10.4 (1991).

[77] S. Hoffmann, R. Koch, and H.-J. Bauer: *Numerical investigation of the low-swirl flow in an aeronautical combustor with angular air supply. Turbo Expo: Power for Land, Sea, and Air*. Vol. 84928. American Society of Mechanical Engineers. 2021.

[78] J. Hertzberg, I. Shepherd, and L. Talbot: *Vortex shedding behind rod stabilized flames*. Combustion and Flame 86.1-2 (1991).

[79] L. Vanquickenborne and A. Van Tiggelen: *The stabilization mechanism of lifted diffusion flames*. Combustion and Flame 10.1 (1966).

[80] S. Marinov, M. Kern, N. Zarzalis, P. Habisreuther, A. Peschiulli, F. Turrini, and O. N. Sara: *Similarity issues of kerosene and methane confined flames stabilized by swirl in regard to the weak extinction limit*. Flow, turbulence and combustion 89.1 (2012).

[81] M. Shamma, S. Hoffmann, S. R. Harth, N. Zarzalis, D. Trimis, R. Koch, H.-J. Bauer, L. Langone, S. Galeotti, and A. Andreini: *Investigation of Adjacent Lifted Flames Interaction in an Inline and Inclined Multi-Burner Arrangement*. *Turbo Expo: Power for Land, Sea, and Air*. Vol. 84959. American Society of Mechanical Engineers. 2021.

[82] M. Shamma, S. Harth, and D. Trimis: *Experimental investigation of multi-burner array with lean lifted spray flames in inline and inclined configurations*. Applications in Energy and Combustion Science 17 (2024).

[83] ARP1533-SAE: *Procedure for the calculation of gaseous emissions from aircraft turbine engines* (1996).

[84] J. C. Wollgarten, N. Zarzalis, F. Turrini, and A. Peschiulli: *Ion current measurements as a method for the detection of the reaction rate in combustion with swirl stabilized airblast injection systems*. *Turbo Expo: Power for Land, Sea, and Air*. Vol. 56758. American Society of Mechanical Engineers. 2015.